THE ASTROPHYSICAL JOURNAL, 421:122–139, 1994 January 20

BRIGHT RADIO CONTINUUM EMISSION FROM STAR FORMATION IN THE CORES OF NEARBY SPIRAL GALAXIES

JEAN L. TURNER
Department of Astronomy, UCLA, Los Angeles, CA 90024
AND
PAUL T. P. HO
Harvard-Smithsonian Center for Astrophysics, 60 Garden Street, Cambridge, MA 02138
Received 1992 November 16; accepted 1993 July 27

ABSTRACT

We have mapped 6 and 2 cm continuum emission from the nuclear regions of ten normal spiral galaxies (Maffei 2, NGC 2403, M81, NGC 4236, NGC 4258, NGC 4736, NGC 4826, M51, M83, and M101) using the VLA. The galaxies were chosen because they are nearby ($\lesssim 5$ Mpc) and likely to have bright continuum emission. Matching beamsizes of $\sim 1\farcs5$ allow the construction of spectral index maps from which the relative amounts of thermal bremsstrahlung and nonthermal synchrotron emission are estimated. Bright radio continuum is detected within the inner arcminute of eight of the 10 galaxies. Even at arcsecond resolution, corresponding to sizescales of 10–30 pc, nonthermal synchrotron emission from supernova remnants (SNRs) dominates the 6 cm continuum fluxes. High intensities suggest that this nonthermal component originates in a large population of young SNRs associated with recent star formation. Candidates for radio supernovae appear in several galaxies, including a candidate for SN 1986L in M83. Weak nonthermal core sources, similar to the Galactic center source Sgr A*, may be present in four of the galaxies. The estimated thermal fluxes indicate that many of the galaxies have significant Lyman continuum fluxes in their cores, $N_{\rm Lyc} \sim 10^{51}$–10^{53} s^{-1}, corresponding to OB luminosities of 2×10^8 $L_\odot$ to 5×10^9 $L_\odot$, generally consistent with observed far-infrared luminosities. Recent star formation appears to dominate both infrared and radio continuum fluxes in these galaxies. We present maps of the separated thermal and nonthermal emission for the starburst sources in Maffei 2 and M83.

Subject headings: galaxies: nuclei — radio continuum: galaxies — supernova remnants

1. INTRODUCTION

The nuclei of normal spiral galaxies are often sites of intense star formation activity. These regions contain as many as 10^3–10^6 OB stars, with star formation rates of up to $\dot{M} \sim 1$ $M_\odot$ yr^{-1}, comparable to that of the entire Milky Way (Scalo 1986; McKee 1989) within regions typically a few hundred parsecs across. Radio continuum maps reveal bright radio continuum emission associated with these regions (Becklin et al. 1980; Rieke et al. 1980; Condon et al. 1982; Ekers et al. 1989), which is largely synchrotron emission. Spectral index measurements suggest that there is also a thermal bremsstrahlung component (Klein & Emerson 1981; Gioia, Gregorini, & Klein 1982; Israel & van der Hulst 1983; Turner & Ho 1983; Condon 1983; Sramek & Weedman 1986; Duric et al. 1986), although there is disagreement as to how much of the emission is thermal.

The advantage of radio continuum emission as a tracer of star formation is that it is impervious to extinction, which is often extremely high, particularly in galactic nuclei. Analysis of the 9.7 μm silicate feature (Lebofsky & Rieke 1979) and Brackett recombination lines (e.g., Roche & Aitken 1985) indicate visual extinctions greater than 20 mag over 100 pc size scales. CO maps suggest that extinctions can be as high as 100 mag over tens of parsec sizescales (e.g., Hurt & Turner 1991). At such high extinctions, even midinfrared observations are affected. Although the extinction may be patchy, allowing some of the optical and infrared emission to escape (van der Hulst et al. 1988), it is advantageous to have a tracer that is unaffected by extinction.

The goals of this study are determination of the morphology of star-forming activity, the Lyman continuum rates, $N_{\rm Lyc}$, and the relation of the synchrotron emission component to the star formation. For nearby galaxies the Very Large Array (VLA)[1] gives resolution sufficiently high that high-brightness emission from H II regions and young supernova remnants (SNRs) can be separated from low-brightness extended synchrotron emission, which dominates single-dish observations. From the spectral index of the emission, relative amounts of bremsstrahlung ("thermal") and synchrotron ("nonthermal") emission can be estimated. In addition to studying the star formation, we are looking for candidates for nuclear activity in the form of unresolved, high-brightness nonthermal nuclear sources similar to the Galactic center source, Sgr A*.

In this study, we focus on the central regions of the nearest large spiral galaxies, Suitable configurations of the VLA at two frequencies give maps with matching beams that allow the construction of spectral index maps. In § 2 we describe the observations; in § 3, the results and thermal separation technique. In § 4 we discuss the sources of the bright continuum emission, in § 5, the star formation properties of the galaxies, and in § 6, the individual galaxies.

2. OBSERVATIONS

The galaxies listed in Table 1 are nearby "normal" spirals showing some evidence of nuclear radio continuum activity, in

[1] The VLA is a facility of the National Radio Astronomy Observatory, which is operated by Associated Universities, Inc., under cooperative agreement with the National Science Foundation.

TABLE 1

RADIO CONTINUUM GALAXY SAMPLE

GALAXY	HUBBLE TYPE	Log $(L_B/L_\odot)$[a]	D (Mpc)	RADIO PEAK[b] α(1950)	RADIO PEAK[b] δ(1950)	RADIO OFFSET[c] ($\Delta\alpha''$)	RADIO OFFSET[c] ($\Delta\delta''$)	T_b PEAK (K)
Maffei 2	SBb	...	5	$02^h38^m08^s.48$	59°23′30″.1	1	3	150
NGC 2403	Scd	9.82	3.2	07 31 56.48	65 43 42.9	56	63	8
NGC 3031 (M81)	Sb	10.31	3.5	09 51 27.33	69 18 08.2	2	5	...
NGC 4236	Sdm	9.45	3.3	12 14 13.864	69 44 40.15	41	−4	45
NGC 4258	Sbc	10.16	5.0	12 16 29.37	47 34 53.1	3	2	25
NGC 4736 (M94)	R Sab	10.07	5.0	12 48 31.89	41 23 31.8	6	4	41
NGC 4826 (M64)	Sab	10.19	5.0	12 54 16.08	21 57 13.1	11	3	15
NGC 5194 (M51)	Sbc	10.38	6.8	13 27 46.335	47 27 10.26	5	6	50
NGC 5236 (M83)	SBc	10.11	3.7	13 34 11.11	−29 36 34.9	5	10	72
NGC 5457 (M101)	Scd	10.37	7.5	14 01 26.27	54 35 17.4	2	2	6

[a] Blue luminosities are from Tully 1987.

[b] Radio peaks and the peak T_b are determined from the uniform 6 cm maps. The accuracy of the absolute radio position depends on the positional accuracy of the phase calibrator, which is $\lesssim$0″.05, signal-to-noise, and source structure.

[c] Offsets are measured from the dynamical centers, when available, from the CO interferometric observations. Errors in these positions are $\lesssim$2″–3″. Otherwise, the nuclear positions are from Dressel & Condon 1976, at accuracy of ±4″. CO positions are from Kenney 1992 (M101); Hurt & Turner 1991 (Maffei 2); Turner, Kenney, & Hurt 1992 (M83).

particular, compact radio continuum emission (van der Hulst, Crane, & Keel 1981, 1983a). Arcsecond resolution corresponds to the size of a classical H II region (~10–30 pc) for these galaxies. High frequency and high resolution maximize our sensitivity to H II regions, which tend to be both spectrally flatter and more intense than standard synchrotron emission sources.

The observations were made at the VLA at 4885 MHz in the B-configuration in 1982 September and October; and at 14965 MHz in the C-configuration in 1983 April. The observations of NGC 2403 are described in Turner & Ho (1983). The weather during all observing sessions was reasonably good. Absolute fluxes were calibrated assuming flux densities for the calibrator 3C 286 of 7.41 Jy at 6 cm and 3.45 Jy at 2 cm and are good to 5%. Phases were calibrated using standard VLA calibration sources. Absolute positional accuracies are 0″.5–0″.1. Phase centers were within 10″ of the peak 6 cm intensities with the exception of NGC 2403 and NGC 4236, which have no detectable nuclear emission.

The maps were made from both naturally weighted (u, v) data, resulting in synthesized beamsizes of ~1″.5, and uniformly weighted data, resulting in beamsizes of ~1″.1. Uniform maps were used for position and brightness temperature measurements, and natural maps were used for display and plots. Galaxies with weaker emission (the extended emission in NGC 4258; NGC 4826; M101) were mapped with Gaussian tapers applied to the (u, v) data resulting in beamsizes as large as 3″–4″. The maps were deconvolved from the dirty beam using the CLEAN algorithm and primary beam corrections were applied. Maffei 2 and M83 were sufficiently strong at 6 cm that a phase-only self-calibration was done. Spectral index maps were formed from the naturally weighted, untapered 6 cm and 2 cm maps after first convolving the maps to strictly identical beamsizes and position angles. In this process, fluxes less than 4 σ were blanked.

The rms noise evels are 0.032–0.043 mJy beam^{-1} for the 6 cm maps and 0.12–0.16 mJy beam^{-1} for the 2 cm maps, corresponding to about one-half hour's integration on each galaxy at each frequency at a bandwidth of 50 MHz. The lowest spatial frequency imposed by the shortest baseline restricts the maps to spatial structures $\lesssim$20″–30″. For this experiment, the high-pass spatial filtering is an advantage since it resolves out extended nonthermal synchrotron emission, allowing us to detect high brightness emission sources such as H II regions or young SNRs.

3. RESULTS

3.1. *Radio Continuum Morphology; Spectral Index Maps*

The 6 cm and 2 cm continuum maps are presented in Figure 1. For each galaxy, the pairs of maps are contoured at the same flux levels, except that the lowest contour, at 3–4 σ, is generally omitted in the noisier 2 cm maps. Positions of the 6 cm intensity peaks are listed in Table 1. For comparison, dynamical centers as determined by interferometric CO observations are also listed. When an accurate dynamical center is not available, we have listed the optical positions of Dressel & Condon (1976). For the purposes of this paper, we are interested in the nuclear emission, although in some cases larger regions have been plotted. Larger scale continuum structure in these galaxies is treated in detail elsewhere (Condon 1983, 1987; Ford et al. 1985; Bash & Kaufman 1986; Tilanus et al. 1988; Duric & Dittmar 1988; Ondrechen 1985).

We detect bright continuum emission in the nucleus, here defined as the inner arcminute, in eight out of 10 galaxies. Only the two smallest spirals in our sample, NGC 4236 and NGC 2403, show no nuclear radio source. The emission is much brighter than that observed in single-dish surveys or lower resolution maps: our 4 σ limit corresponds to ~3 K (0.13 mJy beam^{-1}) at 6 cm and ~1 K (0.6 mJy beam^{-1}) at 2 cm for 1″.5 beams. Peak brightness temperatures are high: 72 K in M83 and 160 K in Maffei 2 at 6 cm, averaging about 20 K in most of the sources. These relatively high intensities limit the possible sources of emission (§ 4).

Morphology is also indicative of the sources of the emission. The complex and extended sources seen in Maffei 2, NGC 4826, M83, the outer "ring" of NGC 4736, and anomalous arms of NGC 4258 are likely to be directly related to recent and vigorous star formation. Supporting this idea is the fact that mid-infrared maps of galaxies are in general remarkably similar to the radio continuum maps (Becklin et al. 1980; Ho et al. 1989; Telesco, Dressel, & Wolstencroft 1993). This correlation may break down at the highest resolutions (Keto et al.

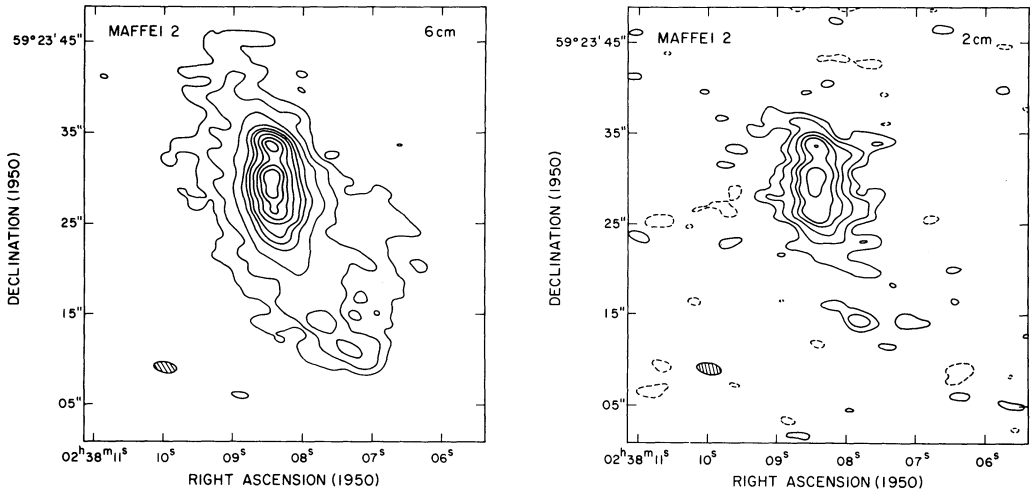

FIG. 1*a*

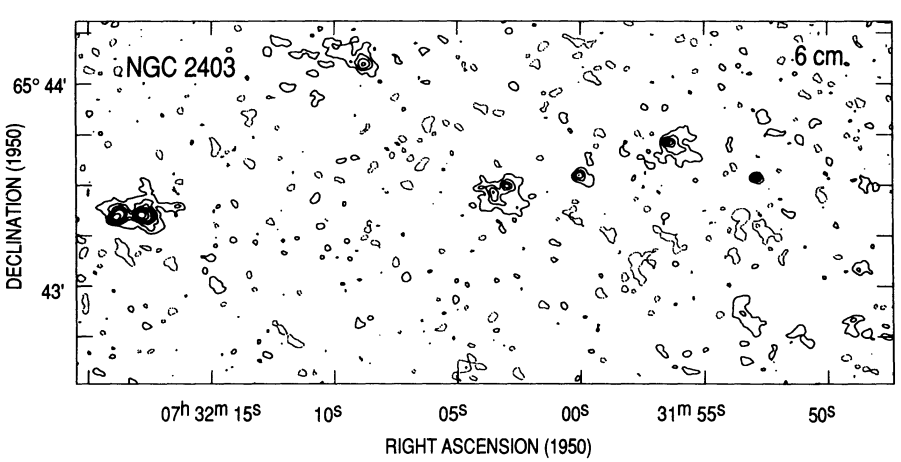

FIG. 1*b*

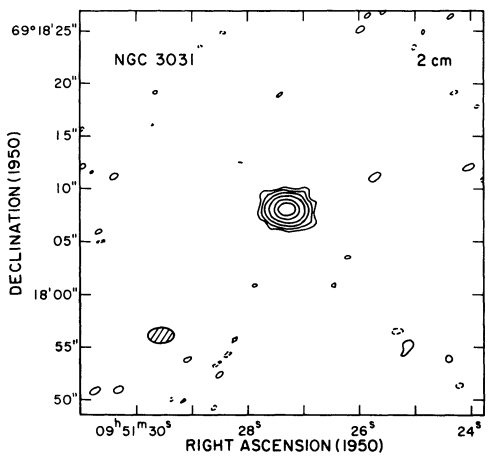

FIG. 1*c*

FIG. 1.—The 6 cm and 2 cm continuum maps. Contour levels and peak flux densities are given separately for each galaxy. Each pair of maps has been convolved to the same beamsize. (*a*) *left*: 6 cm map of Maffei 2. The beamsize is 2.″8 × 1.″5 FWHM, p.a. 79°. Contour levels are ±(0.15, 0.3, 0.6, 1.2, 1.8, 2.4, 3.2, 4.0, 4.8) mJy beam^{-1}. The peak flux density is 8.6 mJy beam^{-1}. *Right*: 2 cm map of Maffei 2. Contour levels are ±(0.4, 0.8, 1.2, 1.6, 2.4, 3.2, 4.0, 4.8) mJy beam^{-1}. Peak flux density is 4.7 mJy beam^{-1}. (*b*) 6 cm map of NGC 2403. The beamsize is 2.″2 × 2.″1, p.a. 23°. Contour levels are ±(0.1, 0.2, 0.3, 0.4, 0.5, 0.7, 1.0) mJy beam^{-1}. The peak flux density is 1.3 mJy beam^{-1}. (*c*) 2 cm map of NGC 3031 (M81). The beamsize is 2.″2 × 1.″6, p.a. 89°. Contour levels are ±(1, 2, 5, 10, 20, 30) mJy beam^{-1}. Peak flux density is 44.3 mJy beam^{-1}. (*d*) *Left*: 6 cm map of NGC 4236. The beamsize is 2.″2 × 1.″8, p.a. −75°. Contour levels are ±(0.25, 0.5, 0.75, 1, 1.5, 2, 3, 4, 5, 6, 7, 8, 9) mJy beam^{-1}. Peak flux density is 3.5 mJy beam^{-1}. *Right*: 2 cm map of NGC 4236. Contour levels begin at 0.5 mJy beam^{-1} and are otherwise as for the 6 cm map. Peak flux density is 6.8 mJy beam^{-1}. (*e*) *Left*: 6 cm map of the nucleus of NGC 4258. Beam is 3.″7 × 2.″8, p.a. 75°. Contour levels are ±(0.15, 0.3, 0.45, 0.6, 0.9, 1.2, 1.8, 2.4, 3.0) mJy beam^{-1}. Peak flux density is 2.1 mJy beam^{-1}, *Right*: 2 cm map of NGC 4258. Contour levels begin at 0.6 mJy beam^{-1} and otherwise are the same as for the 6 cm map. Peak flux density is 3.2 mJy beam^{-1}. (*f*) 6 cm map of the inner 2 kpc of NGC 4258. The map is tapered to bring out slightly more extended, low-brightness structure. Beam is 3.″1 × 2.″8, p.a. −82°. Contours are the same as for the higher resolution 6 cm map in (*e*). Note the weak emission along the "anomalous" Hα and radio continuum arms in a spiral pattern to the northwest and southeast of the nucleus. The strong point source to the north of the nucleus is a radio supernova. (*g*) *Left*: 6 cm map of NGC 4736. Beam is 3.″9 × 3.″7, p.a. −85°. Beam is 1.″9 × 1.″6, p.a. 81°. Contour levels are ±(0.2, 0.4, 0.6, 0.8, 1, 1.2, 1.6, 2, 2.4, 3.2, 4) mJy beam^{-1}. Peak flux density is 4.6 mJy beam^{-1}. *Right*: 2 cm map of NGC 4736. Contour levels begin at ±0.6 mJy beam^{-1}. Peak flux density is 2.4 mJy beam^{-1}. (*h*) *Left*: 6 cm map of NGC 4826. Beam is 2.″4 × 2.″3, p.a. −55°. Contour levels are ±(0.12, 0.24, 0.36, 0.48, 0.60, 0.72, 0.96, 1.2) mJy beam^{-1}. Peak flux density is 1.7 mJy beam^{-1}. *Right*: 2 cm map of NGC 4826. Contour levels begin at 0.36 mJy beam^{-1} and otherwise are the same as for the 6 cm map. Peak flux density is 0.8 mJy beam^{-1}. (*i*) *Left*: 6 cm map of M51. Beam is 2.″4 × 1.″7, p.a. 87°. Beam is 2.″ × 2.″4, p.a. 86°. Contour levels are ±(0.15, 0.3, 0.45, 0.75, 1.05) mJy beam^{-1}. Peak flux density is 1.4 mJy beam^{-1}. *Right*: 2 cm map of M51. Contour levels begin at 0.45 mJy beam^{-1} and otherwise are as for the 6 cm map. Peak flux density is 1.3 mJy beam^{-1}. (*j*) *Left*: 6 cm map of M83. Beam is 3.″4 × 2.″4, p.a. 1°. Contour levels are ±(0.3, 0.6, 1.2, 1.8, 2.4, 3.6, 4.8, 6.0, 7.2) mJy beam^{-1}. Peak flux density is 8.81 mJy beam^{-1}. *Right*: 2 cm map of M83. Contour levels begin at ±0.6 mJy beam^{-1}, otherwise are the same as for the 6 cm map. Peak flux density is 5.7 mJy beam^{-1}. (*k*) 6 cm map of M101. Beam is 2.″4 × 2.″1, p.a. −78°. Contour levels are ±(0.12, 0.16, 0.2, 0.24, 0.28) mJy beam^{-1}. Peak flux density is 0.63 mJy beam^{-1}.

1993), probably because the individual star-forming regions are being resolved.

The radio continuum morphology in these galaxies often consists of coherent structures of ~100 pc to ~1 kpc in extent. Dynamical crossing times for these structures are far longer than the lifetimes of massive young stars, or even than the expected duration of a particular episode of star formation. Thus the existence of these structures is likely to have an external cause, which is probably the distribution of molecular gas. For example, the "barlike" distribution of the continuum emission in the center of Maffei 2 is extremely well correlated with the distribution of molecular gas (Ishiguro et al. 1989; Hurt & Turner 1991). The correlation of the molecular gas and the radio continuum emission is probably due to enhanced star formation along spiral arms, although magnetic field compression in density waves (Mathewson, van der Kruit, & Brouw

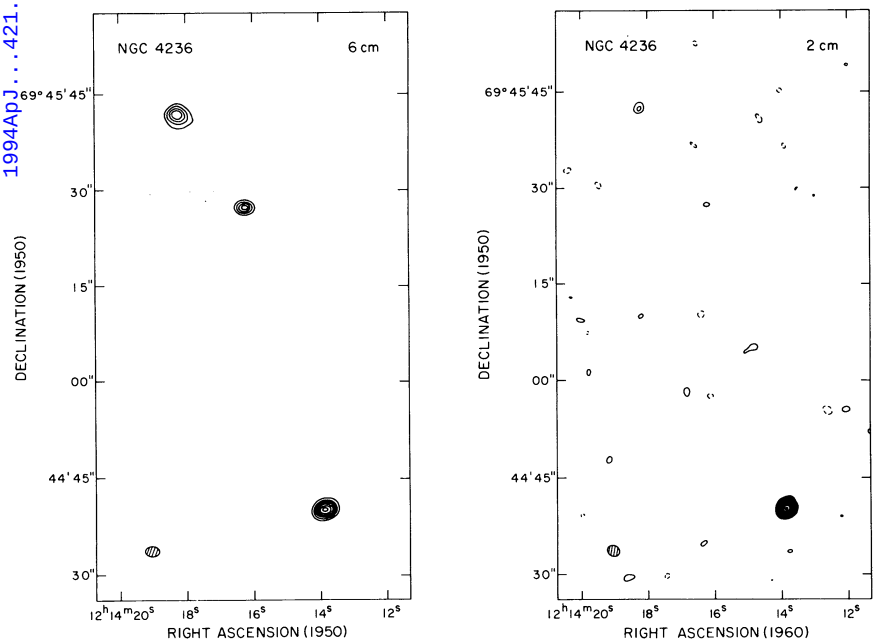

FIG. 1*d*

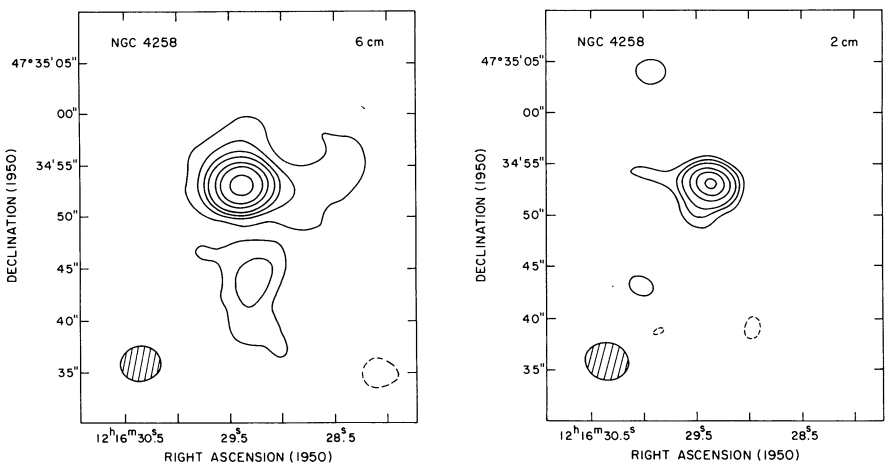

FIG. 1*e*

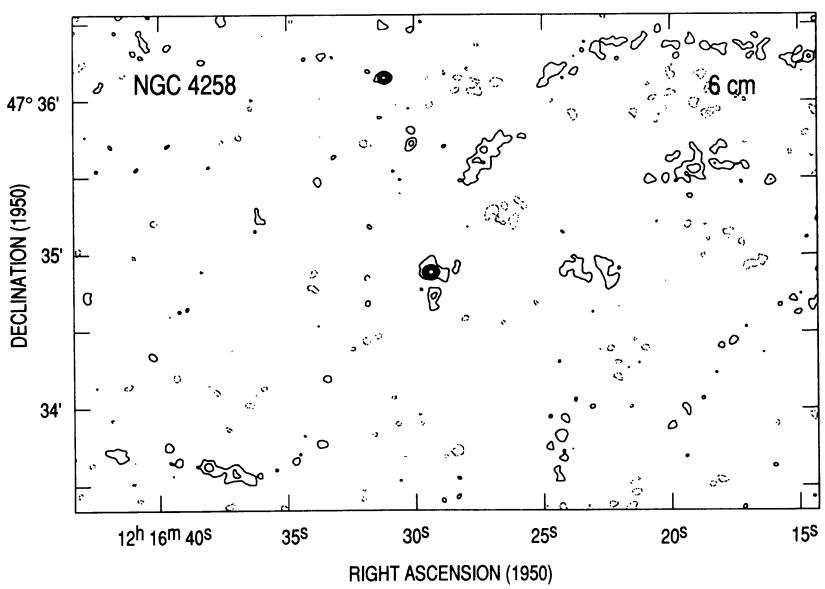

FIG. 1*f*

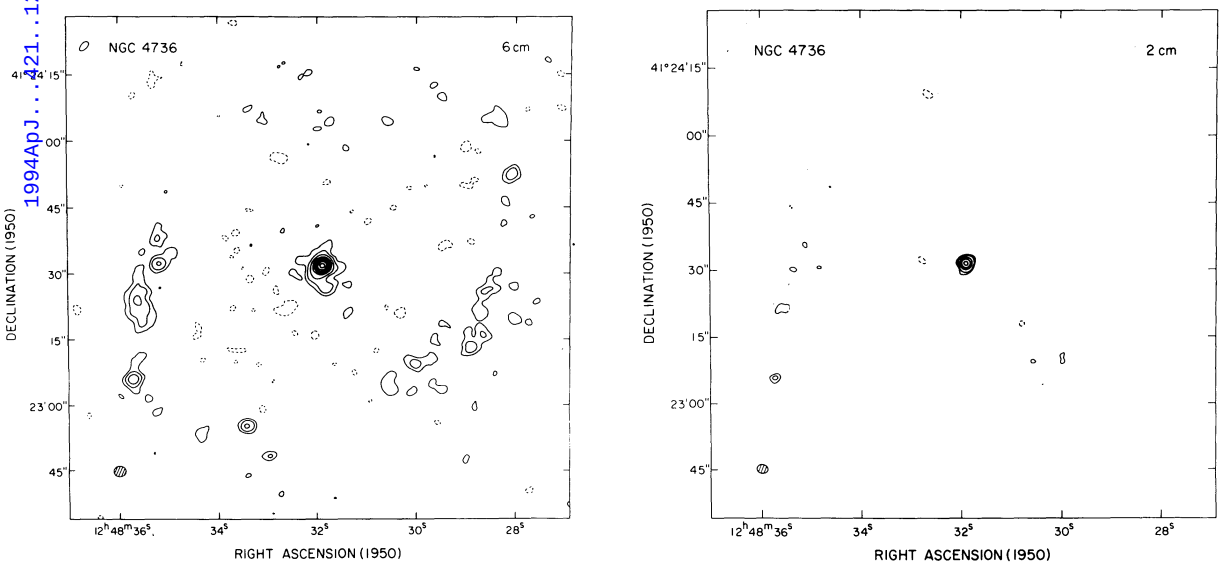

FIG. 1*g*

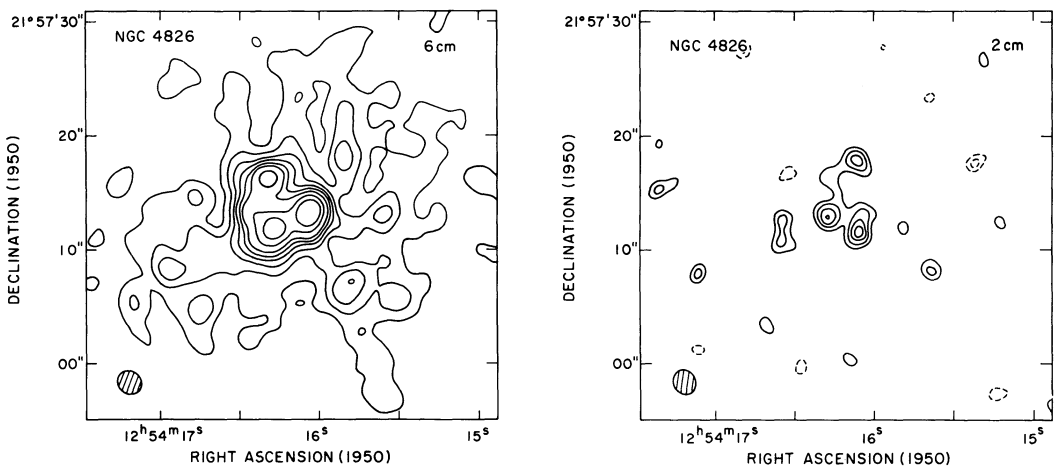

FIG. 1*h*

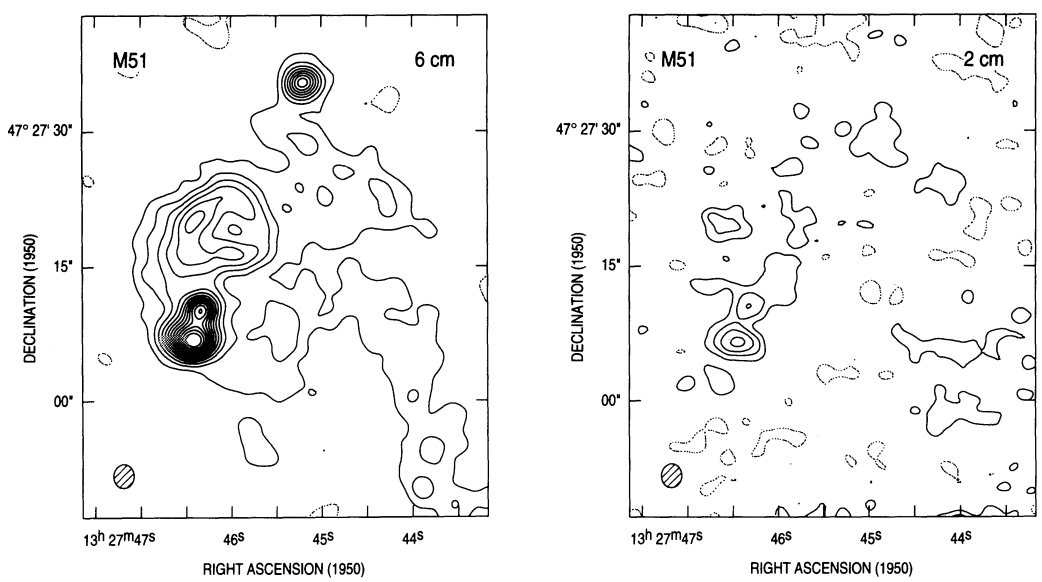

FIG. 1*i*

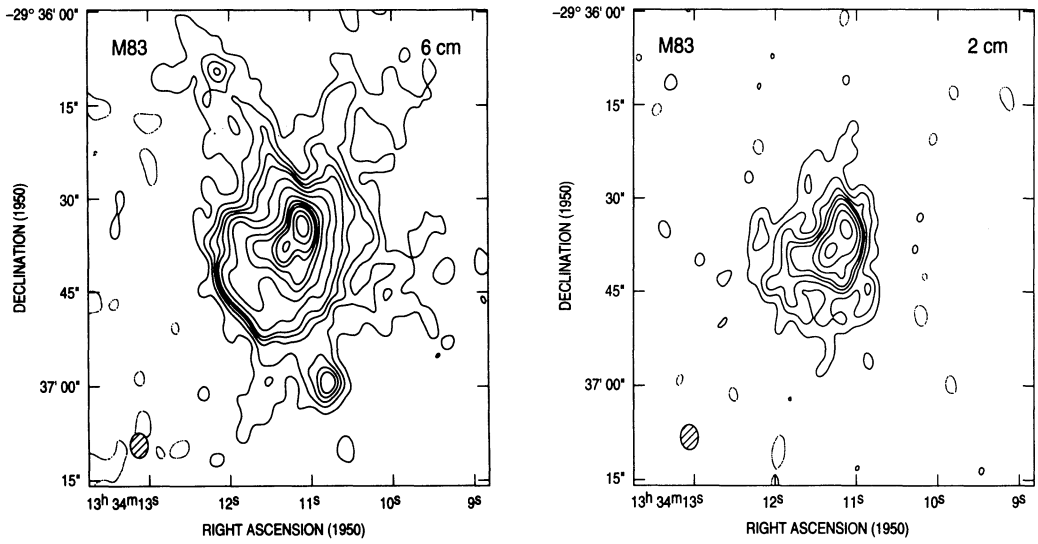

FIG. 1*j*

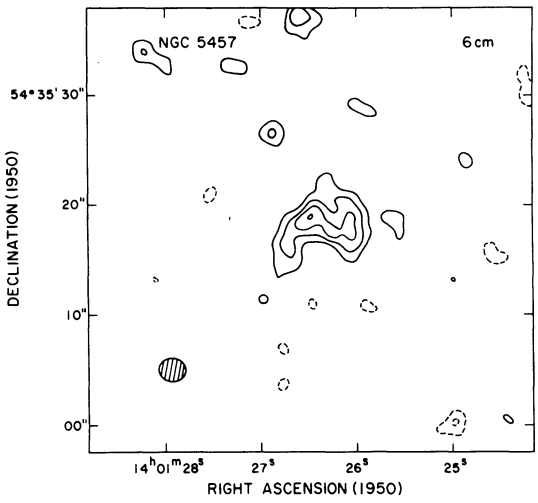

FIG. 1*k*

1972; Visser 1980; Duric 1986a, b), or elevated cosmic ray heating of the clouds in the arms (Adler, Allen, & Lo 1991), may also enhance radio continuum there.

Although the continuum emission is often extended, there are always compact components within the extended emission. Compact structures are particularly evident in Maffei 2, NGC 4826, NGC 4736, M51, and NGC 4258 (Figs. 1*a* and 1*e*–1*i*). Since undersampled emission often resembles point sources, particularly in a CLEANed image, identification of compact sources embedded in extended emission requires some judgment. We have listed compact sources in Table 2. These sources have peak flux densities greater than 6 σ and to appear to be real structures due to either their isolation, their appearance in both 6 cm and 2 cm maps, or idiosyncratic spectral index. Where the existence of a compact source is less certain, it is marked "extended." We expect that some of these sources may be variable radio supernovae (§ 4.1); these sources have been marked "RSN". In some cases (e.g., NGC 4258 nuclear source), positions may differ from those listed in Table 1, since the peaks are resolution dependent, and the maps used for Table 2 are often tapered or naturally weighted.

In M81, NGC 4258, NGC 4736, and M51 there are bright, compact continuum sources located very close to the dynamical centers. These sources are unresolved and all have brightness temperatures of $T_b \gtrsim 500$ K, as determined by deconvolving a Gaussian source from the beam. The fact that the brightest sources are located at the very centers of the galaxies is probably not a coincidence. Except for M81, which has a well-known active nucleus (Kellerman et al. 1976), these lower limits to T_b do not rule out H II regions as a source of this emission. However, the proximity of these sources to the nucleus and their small sizes strongly suggest that these are "core" sources similar to the Galactic center source, Sgr A*. Confirmation of this conjecture requires higher resolution. In most of these sources there is spectroscopic evidence for nuclear activity as well (§ 6.3). We have listed the possible core sources in Table 3; their positions are listed in Table 1.

To determine approximately how much extended emission is missing from the VLA maps due to undersampling, we compare the total fluxes in the VLA maps to single-dish fluxes. In Table 4 we list total mapped fluxes for the inner arcminute of the fields and single-dish fluxes from the literature. With the exception of M101, the inner arcminute contains most of the bright continuum emission within the 9′ diameter of the 6 cm VLA primary beam for these galaxies. In general, about one-half of the single-dish radio flux at these frequencies on 1′–3′ size scales is contributed by an extended ($\gtrsim$20″–30″), low-brightness component that does not appear in these maps. We note that because the 6 cm and 2 cm maps were obtained with matched VLA configurations, they have the same (u, v) coverage and are sensitive to the same spatial scales.

The spectral indices of the single-dish emission and the compact emission of the VLA maps are very different. This suggests that these two techniques measure components that are intrinsically different. Spectral indices, defined as $S_\nu \propto \nu^\alpha$, are listed in Table 4. With this convention, thermal emission has positive or flat spectral index, while synchrotron emission is negative. Single-dish spectral indices at these wavelengths are remarkably uniform at $\alpha \sim -0.6$ to -0.8 (Klein & Emerson 1981; Wunderlich, Klein, & Wielebinski 1987; Gioia et al. 1982). (The exceptions are M81 and NGC 4736, in which the nuclear fluxes are dominated by compact nuclear sources [§ 6.3].) The extended radio continuum disk component appears more uniform from galaxy to galaxy than the compact emission component. The disk component is responsible for

TABLE 2

COMPACT CONTINUUM SOURCES

Source	α(1950)	δ(1950)	S_6[a] (mJy beam^{-1})	S_6^{tot}[b] (mJy)	S_2[a] (mJy beam^{-1})	S_2^{tot}[b] (mJy)	α[c]	Comments
Maffei 2:								
Beam: 2.″0 × 1.″0, 85°								
1	02^{h}38^{m}07.^{s}38	59°23′11.″1	0.5	1.0	<0.3	...	< −0.4	
2	07.8	14	0.7	...	0.8	...	−0.1	6 cm peak. 2 cm peak is 1″ E
3	08.44	26.4	4.0	...	1.9	...	−0.6	
4	08.44	28.3	5.6	...	2.1	...	−0.9	
5	08.48	30.1	6.2	...	2.3	...	−0.9	
6	08.44	33.6	4.7	...	2.4	...	−0.6	
7	08.95	21.3	0.2	...	0.9	...	+0.9	
NGC 2403:								
2.″2 × 2.″1, 23°								
1	07^{h}31^{m}30.^{s}47	65°43′43.″8	0.4	6.4	...	...	...	Shell source of diameter 7″
2	52.88	32.4	0.5	0.5	...	...	...	RSN?
3	56.48	42.9	0.5	4.6	...	...	...	
4	32 00.03	33.0	0.4	1.3	...	...	...	RSN?
5	03.05	29.7	0.4	6.9	...	...	...	
6	08.84	44 05.4	0.3	10.9	...	...	...	
7	17.84	43 21.2	1.3	10.6	...	...	...	Double source: total flux is for both
	18.91	20.3	0.7		...	...	...	(background galaxy?)
NGC 4236:								
2.″2 × 1.″8, −75°								
1	12^{h}14^{m}13.^{s}864	69°44′40.″15	3.5	3.8	6.8	6.8	+0.6	
2	16.23	45 27.3	1.3	1.3	<0.3	...	< −1.3	RSN?
3	18.245	41.75	1.6	3.0	0.8	2	−0.6	RSN?
NGC 4258:								
3.″6 × 2.″8, −82°								
1	12^{h}16^{m}14.^{s}56	47°36′16.″8	0.3	...	...	...	...	
2	19.1	35 33	0.4	...	...	...	...	
3	23.6	34 56	0.3	...	...	...	...	Extended
4	22.9	36 20	0.3	...	...	...	...	
5	24.3	33 49	0.3	...	...	...	...	Extended
6	24.6	36 11	0.3	...	...	...	...	
7	27.31	35 40.6	0.4	...	...	...	...	
8	27.6	35 37	0.3	...	...	...	...	Extended
9	29.27	34 43.9	0.3	...	0.3	0.3	0	On CO ridge
10	29.39	34 53.20	2.1	2.4	3.2	3.2	+0.4	Nuclear source
11	30.10	35 43.3	0.4	1.0	...	...	...	
12	31.199	36 09.10	0.9	1.1	...	...	...	SN 1981K
13	33.69	33 46.0	0.2	...	...	...	...	
14	37.0	33 34	0.3	...	...	...	...	Extended
15	38.1	33 38	0.4	...	...	...	...	Extended
NGC 4736:								
1.″1 × 1.″0, −83°								
1	12^{h}48^{m}28.^{s}5	41°24′06″	0.2	1.2	0.4	...	+0.6	
2	28	52	0.3	0.7	0.4	0.9	+0.3	
3	28.6	26	0.2	3.0	<0.4	...	< +0.5	Extended
4	28.9	13	0.3	3.4	0.5	0.9	+0.5	Extended
5	30	9	0.3	1.9	0.4	...	+0.3	DD source 15
6	31.4	21	0.2	0.4	<0.2	...	<0	DD source 13
7	31.83	26.5	0.4	...	<0.1	...	< −1.0	
8	31.88	31.9	3.6	6.1	...	...	...	Nuclear source–6 cm
	31.9	31.4			2.4	3.2	−0.3	Nuclear source–2 cm
9	32.9	22 48	0.3	0.4	<0.3	...	<0	
10	33.410	55.19	0.4	0.6	<0.3	...	< −0.3	RSN?
11	34.4	53	0.2	0.8	<0.3	...	< +0.4	
12	35.2	23 32	0.4	0.8	0.3	...	−0.3	
13	35.6	24	0.4	2.7	0.3	2.8	−0.3	
14	35.722	06.04	0.6	0.9	0.7	1.2	+0.1	RSN?
NGC 4826:								
2.″4 × 2.″3, −55°								
1	12^{h}54^{m}15.^{s}81	21°57′06.″8	0.2	...	0.2	...	0.0	
2	16.08	13.1	1.7	...	0.5	...	−1.1	RSN?
3	16.09	11.7	0.7	...	0.8	...	−0.1	
4	16.11	18.0	0.4	...	0.7	0.7	+0.5	
5	16.29	12.0	1.4	...	0.6	...	−0.8	RSN?
6	16.32	15.9	1.1	...	0.4	...	−0.8	RSN?
7	16.6	11	0.4	...	0.5	1.0	+0.2	
8	17.10	07.8	0.4	...	0.5	0.5	+0.2	
9	17.3	15	0.4	...	0.5	2.1	+0.2	

TABLE 2—*Continued*

Source	α(1950)	δ(1950)	S_6[a] (mJy beam^{-1})	S_6^{tot}[b] (mJy)	S_2[a] (mJy beam^{-1})	S_2^{tot}[b] (mJy)	α[c]	Comments
M51								
2″.9 × 2″.4, 86°								
1	13^{h}27^{m}45^s.202	47°27′35″.49	1.1	1.8	0.2	...	−1.5	RSN?
2	46	20	0.7	14	...	6	< −0.8	Large shell
3	46.335	10.26	1.4	2.3	0.7	1.6	−0.6	Core source?
4	46.4	0.7	1.5	3.6	1.3	2.2	−0.1	Southern "jet"
M83								
2″.5 × 1″.6, 3°								
1	13^{h}34^{m}10^s.80	−29°36′59″.4	0.5	...	0.3	...	−0.5	
2	11.11	34.9	5.4	...	4.5	...	−0.2	SN 1968L? See text.
3	11.15	41.5	2.3	...	2.3	...	0	Extended
4	11.30	38	3.7	...	3.6	...	−0.2	
5	11.56	38	2.0	...	1.3	...	−0.4	2 cm peak
6	11.74	38.3	1.5	...	1.5	...	0	2 cm peak
7	11.8	45	1.1	...	1.0	...	−0.1	Extended

[a] Peak flux densities in this table are generally computed from the naturally weighted maps. The tabulated flux densities may therefore differ from peaks in Table 1 or Fig. 1, which are often from uniformly weighted (Table 1) or tapered maps. For this reason, synthesized beams are listed beneath the source name.

[b] Flux densities are for compact components only. Where there is significant extended emission, a flux is not computed.

[c] Spectral indices are computed from the peak flux densities.

TABLE 3

SUSPECTED CORE SOURCES

Galaxy	Core Flux (mJy) 6 cm	Core Flux (mJy) 2 cm	α	Deconvolved Size	T_b (6 cm) (K)	L_6 (10^2 $L_\odot$)
M81	92	45	−0.6	0.36 × 0.16	81000	1000
NGC 4258	1.8	3.1	+0.5	0.45 × 0.16	1300	0.7
NGC 4736	3.6	2.2	−0.4	0.63 × 0.27	1100	1.4
M51	1.1	<1.0	< −0.9	0.75 × 0.16	460	0.8

NOTE.—Fluxes are derived from uniform, self-calibrated maps and represent the total source flux, not the peak. The 6 cm M81 flux is from Bash 1986. Sizes, fluxes, and brightness temperatures are from deconvolved source parameters assuming a Gaussian source structure. The deconvolved sizes are likely to be lower limits to the true core sizes, with the limitation being phase noise.

TABLE 4

RADIO CONTINUUM FLUXES

Galaxy	Single Dish Flux[a] (mJy) 6 cm	Single Dish Flux[a] (mJy) 2 cm	α_{ave}	Total Mapped Flux[b] (mJy) 6 cm	Total Mapped Flux[b] (mJy) 2 cm	α_{mapped}	Estimated Thermal Flux[b] (mJy) 6 cm	Estimated Thermal Flux[b] (mJy) 2 cm	L_6^{nt}[c] (3×10^{17} W Hz^{-1})
Maffei 2	260	100	−0.9	107	46	−0.8	20	18	870
NGC 2403	120	55	−0.7	<1	...[d]	...[d]	<1	...	<4
M81	100	90	~0	92[e]	45	−0.6	...	...	1900
NGC 4236	<40	<40	...	9	11	+0.2	<1	<1	40
NGC 4258	273	140	−0.6	10	6	−0.5	2	2	80
NGC 4736	110	80	−0.3	11	9	−0.2	2	2	90
NGC 4826	60	25	−0.8	29	9	−1.1	1	1	280
M51	360	190	−0.6	46	17	−0.9	5	4	720
M83	490	155	−1.0	180	78	−0.8	50	45	710
M101	290	120	−0.8	3	...[d]	...[d]	≤3	<3	<35

[a] Klein & Emerson 1981, except as noted below. 15 GHz fluxes are extrapolated from their 10.7 GHz fluxes and spectral indices. The beam of the 100 m telescope is 70″ at 10.7 GHz. Other single dish references: Maffei 2 at 6 cm, Seaquist, Pfund, & Bignell 1976; NGC 4236, extrapolated from 11 cm data of de Jong 1967; NGC 4736 at 6 cm, de Bruyn 1977; NGC 4826 and M51 at 6 cm, Sramek 1975; M83, Whiteoak 1970 (6 cm), Ekers et al. 1989 (2 cm).

[b] Mapped fluxes correspond to the central 1′ of the primary beam, excluding structures ≲30″ across, for sources with intensities ≲0.5 mJy beam^{-1}. Thermal fluxes exclude possible "core" sources (Table 3).

[c] Estimated nonthermal luminosities.

[d] Not observed at 2 cm.

[e] Bash 1986. The M81 nuclear source is variable, which may explain the difference between the single dish and VLA spectral index.

the well-known infrared-radio continuum correlation revealed by the *IRAS* data (Dickey & Salpeter 1984; de Jong et al. 1985; Helou, Soifer, & Rowan-Robinson 1985; Gavazzi, Cocito, & Vettolani 1986). Since the extended component originates in cosmic rays diffusing through the interstellar medium (ISM) it is likely to reflect the long-term global star-formation history of the galaxy.

By contrast the spectral indices for the VLA fluxes vary significantly. This is particularly evident in the individual sources listed in Table 2, which range from $\alpha = +0.4$ in the compact nuclear source of NGC 4258 to -1.0 in the extended source in NGC 4826. Spectral index maps for the most complex sources are presented in Figure 2 as gray-scale plots superposed on contour plots of the 6 cm continuum. Darker shades represent flatter, more thermal emission. It is clear that the 6 cm continuum emission in these galaxies is everywhere dominated by nonthermal emission, even on size scales of tens of parsecs. Since these are normal spiral galaxies, the nonthermal emission is probably due to cosmic rays originating in SNRs (Caesarsky 1980), particularly relatively young ones associated with recent star formation (§ 4.1). Aside from the unresolved "core" sources, it is unlikely that the emission in these galaxies is due to nuclear activity, with the possible exceptions of M51 and NGC 4258 (§ 6.3).

3.2. *Separation of Thermal and Nonthermal Fluxes*

Relative amounts of thermal and nonthermal emission can be estimated from these maps by exploiting differences in spectral index (e.g., Turner & Ho 1983). Given the thermal spectral index, α_t, and the nonthermal index, α_{nt}, the 6 and 2 cm maps can be combined to produce maps of the thermal and nonthermal emission at either frequency.

For the spectral separation, we assume that the SNR and H II regions have properties similar to their Galactic counterparts. On spatial scales larger than 10 pc, H II regions at 6 cm and 2 cm are almost always optically thin, or close to it, so we adopt $\alpha_t = -0.1$. Nonthermal synchrotron emission has a larger range of spectral index. Galactic SNR have spectral indices of $\alpha_{nt} \sim -0.6$ to -0.2, with the vast majority in the range -0.5 to -0.4 (Green 1984; Mills et al. 1984; Weiler et al. 1986). Extended synchrotron disk emission has spectral index $\alpha_{nt} \sim -1.0$ in the Galaxy (Salter & Brown 1988) and $\alpha_{nt} \sim -0.8$ to -0.6 in nearby galaxies (Klein & Emerson 1981; Gioia et al. 1985; Wunderlich et al. 1987). This range is consistent with the extended emission in our spectral index maps. In spite of the uncertainty in α_{nt}, it is possible to separate the thermal from the nonthermal emission with reasonable accuracy at these spatial resolutions, contrary to what has previously been claimed (Wynn-Williams & Becklin 1985). This is because α_{nt} is nearly always significantly more negative than α_t.

For each map pixel, the thermal flux, S_6^t, and nonthermal flux, S_6^{nt}, were calculated from the observed 6 cm and 2 cm fluxes, S_6 and S_2, using

$$S_6^t = [S_2 - S_6(\nu_2/\nu_6)^{\alpha_{nt}}][(\nu_2/\nu_6)^{\alpha_t} - (\nu_2/\nu_6)^{\alpha_{nt}}]^{-1} ,$$

and $S_6^{nt} = S_6 - S_6^t$. We assume that α_t and α_{nt} are constant across the map. For α_t this is an excellent approximation. For α_{nt} there is no a priori value, so for each galaxy we made separated maps using values for α_{nt} of -0.5 to -0.8, at 0.1 intervals. The best choice for α_{nt} was deemed to be that which maximized the fluxes in both maps. Best fit α_{nt} were ~ -0.6 to -0.8. We found that the variation in S_6^t and S_6^{nt} was relatively insensitive to choice of α_{nt}. The derived thermal fluxes varied by less than $\lesssim 30\%$ for the given range of α_{nt}, for the strongest sources. For the weakest sources, ($S_6^t < 2$–3 mJy), imperfect CLEANing of extended nothermal emission generally becomes important and the fluxes are only accurate to a factor of two. The maps of the separated thermal and nonthermal emission are discussed in detail for the complex sources in M83 and Maffei 2 in § 6.2; thermal and nonthermal maps have also been produced for NGC 253 (Turner & Ho 1985).

Other sources of error in the separation aside from the unknown and variable α_{nt} include the presence of plerions such as the Crab nebula. The relatively flat spectral indices of plerions ($\alpha_t = -0.2$ to -0.3) would result in some portion of the plerion flux being attributed to S_6^t. However since there are only one-half dozen known plerions in the Galaxy, their individual fluxes would be $\lesssim 1$ mJy at Mpc distances, and only a fraction of this flux would be separated as "thermal." Hence, we expect plerions to contribute at most a few percent to the estimated thermal fluxes.

4. SOURCES OF BRIGHT RADIO CONTINUUM EMISSION IN NORMAL SPIRAL GALAXIES

The sources of the bright radio continuum emission in normal spirals can be spectrally classified as thermal bremsstrahlung or nonthermal synchrotron emission. However, spatial structure and brightness temperature further constrain the possible emission sources. In particular, the emission in these VLA maps can originate only in the brightest radio sources, such as H II regions or relatively young SNR.

4.1. *Sources of Bright Nonthermal Emission: SNR and RSN*

Synchrotron emission dominates the radio continuum emission from normal spiral galaxies. Synchrotron emission disk emission is produced by cosmic rays diffusing along the galactic magnetic field (e.g., Salter & Brown 1988; Duric 1986b). The "disk" component is dominant in lower resolution and lower frequency maps (e.g., Hummel et al. 1985; Condon 1987). The maps of this study are not sensitive to the disk component. Westerbork maps show that typical intensities for disk emission are $T_b \lesssim 0.1$–0.2 K at 6 cm (Ekers 1975; van der Kruit 1973a, b, c), about a factor of 10 below our detection limit. Even enhanced emission in the spiral arms is visible only at the lowest levels in these maps (Figs. 1*f*, 1*g*, and 1*i*). The disk component will be at least an order of magnitude fainter at 2 cm and is therefore not present in the 2 cm maps.

Aside from the active galactic nucleus (AGN) candidates of Table 3, the only synchrotron sources that are sufficiently bright to appear in these maps are either large complexes of relatively young radio SNRs or radio supernovae (RSNs). The distinguishing feature between SNRs and RSNs is timescale: RSNs are the bright, rapidly evolving ($t_{1/2} \sim 50$ yr) synchrotron sources associated with optical supernovae (Weiler et al. 1986, 1989; Weiler & Sramek 1988; Sramek & Weiler 1990) and are presumably the result of the interaction of a blast wave with a dense stellar wind remnant (Chevalier 1982). Radio SNR are "standard" remnants associated with the Sedov phase in a diffuse ($n_0 \lesssim 1$ cm^{-2}) ISM, which appear a few hundred yr after the supernova and remain as distinguishable entities for $\sim 10^3$–10^4 yr. Since the lifetimes and general properties of these two classes of radio remnants are distinctive, we will distinguish between SNRs and the shorter lived RSNs, although their origins may be similar.

The observed range of intensities at 6 cm, T_b(6 cm) $\sim$ 1–90 K, is consistent with either SNR of diameter >20 pc, or complexes

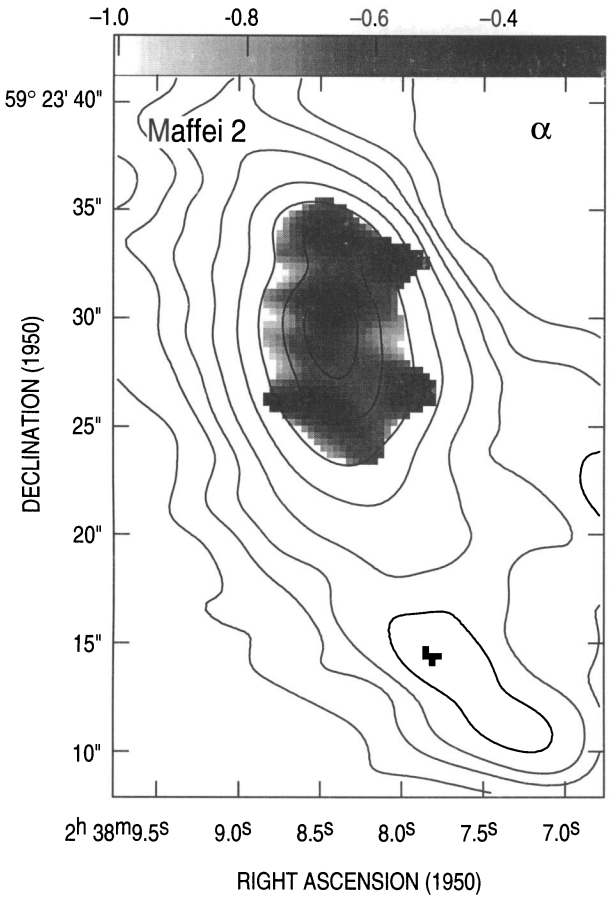

FIG. 2*a*

FIG. 2.—Spectral index maps. Gray scale is spectral index defined as $S \propto \nu^{\alpha}$; the gray-scale range is -1.0 to $+0.3$. Overlaid on the spectral index maps are the 6 cm contours. The spectral index maps are clipped for fluxes less than 3 σ, which is 0.016 mJy beam^{-1} for 6 cm and 0.5 mJy beam^{-1} for 2 cm; since the 2 cm maps are noisier, the outlines of the spectral index maps usually reflect the 3 σ levels of the 2 cm map. Strong positive spectral indices at the edges of the maps can be caused by undersampling at 6 cm, noise bias, or CLEAN problems. The spectral index maps are only reliable in the high signal-to-noise central portions of the maps. Beams are as in Fig. 1: (*a*) Maffei 2, (*b*) NGC 4826, (*c*) M51, and (*d*) M83.

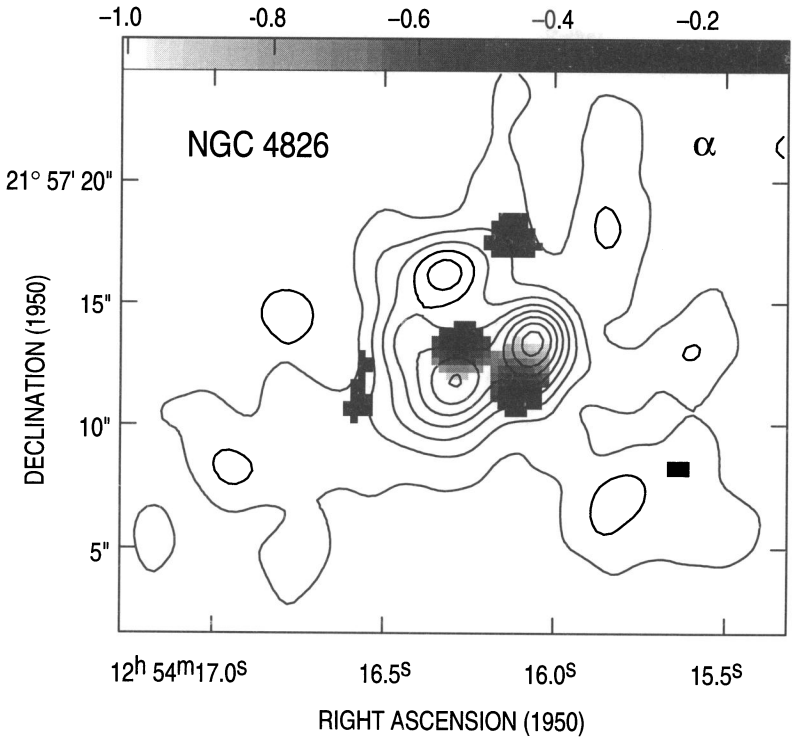

FIG. 2*b*

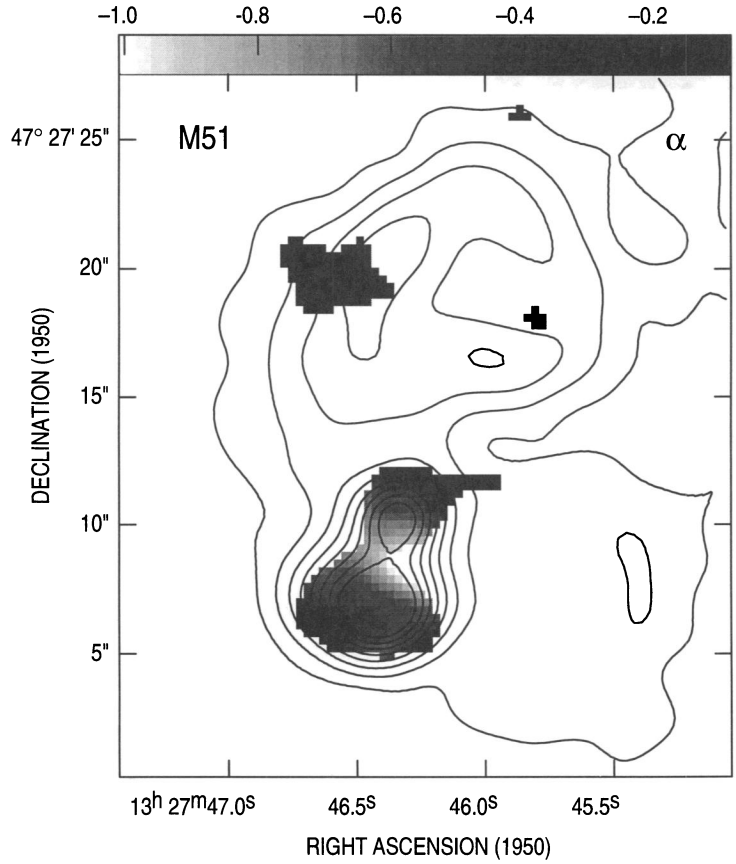

FIG. 2*c*

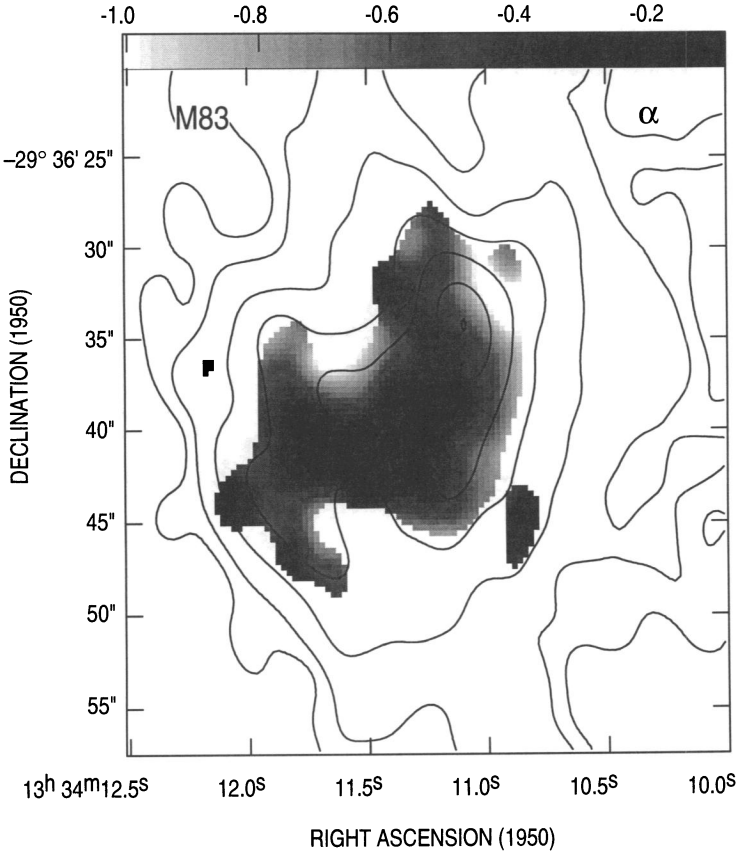

FIG. 2*d*

of bright, young SNRs. Individual young SNRs, such as Cas A, have high intrinsic brightness temperatures but low antenna temperatures because they are so much smaller than the beam. The antenna temperature of Cas A, which has a diameter of 3 pc and $T_b \sim 1000$ K at 6 cm (Goss, Kalberla, & Dickel 1984) is beam-diluted to ~ 10 K $(D/3.2\ \mathrm{Mpc})^{-2}(\theta_B/2'')^{-2}$. Cas A would be detectable at 6 cm out to 5 Mpc. However, Cas A is one order of magnitude brighter than typical young SNR. Larger SNR are far less intense [T_b(6 cm) $\sim$ 5–10 K, Clark & Caswell 1976; Mills et al. 1984; Green 1984] but are consistent with the observed brightnesses since they will fill the 20–30 pc beams. However, they cannot explain the brightest sources in Maffei 2 or M83.

At 2 cm, the observed intensities, T_b(2 cm) $\sim$ 1–10 K, rule out most Galactic-type SNR sources. Even Cas A would have $T_b < 0.2$ K at the distance of our closest galaxy (Cas A flux from Baars et al. 1977). Larger SNRs ($D > 20$ pc) have intensities of <0.1 K. Much of the emission in the 2 cm maps is therefore likely to be thermal. In fact, the thermal map separations closely resemble the 2 cm maps. H II regions are also consistent with the more compact nature of the 2 cm emission.

RSNs are bright enough to produce the observed intensities in either the 6 cm or 2 cm maps but are not likely to dominate the observed total fluxes, particularly at 6 cm. Kronberg, Biermann, & Schwab (1985) speculate that the twenty-some bright point sources in M82 are RSNs, and the angular sizes of the sources are consistent with this interpretation (Bartel et al. 1987). Mean fluxes for the brightest 10 sources in M82 are ~ 8 mJy at 6 cm and 7 mJy at 2 cm, with median values of 2–3 mJy at both 6 cm and 2 cm. These would be easily detectable in our sample galaxies. However, since the half-lives of RSNs are so short, $t_{1/2} \lesssim 50$ yr (Weiler & Sramek 1988; Sramek & Weiler 1990), for RSNs to constitute a significant fraction of the mapped fluxes in these galaxies, supernova rates of $\gtrsim 1\ \mathrm{yr}^{-1}$ are required. In M82, the supernova rate may be high enough. But for the galaxies of the present study, such high supernova rates are generally inconsistent with observed infrared luminosities (§ 5).

4.2. *Sources of Thermal Emission:* H II *Regions*

The high brightness limit of this survey is amenable to H II regions since they are intrinsically bright. Even so, our flux density and brightness limits filter out all but the most energetic H II regions.

Compact H II regions are optically thick and therefore very bright, with $T_b = T_e = \sim 5000$–10000 K, far above our 1 K brightness limit. However they are severely beam-diluted. For electron temperatures of 8000 K, individual compact H II regions will have brightness temperatures of $T_b \sim 0.1$ K $(d/0.1\ \mathrm{pc})^2\ (D/3.2\ \mathrm{Mpc})^{-2}$ (Habing & Israel 1979) and are therefore not detectable here. However, clusters of compact H II regions exceeding ~ 0.5 pc in diameter would be.

"Classical" H II regions of moderate size (~ 10 pc) are also detectable. Although optically thin, they are sufficiently bright and extended to be detectable. For resolved H II regions, we can detect emission measures of EM $> 8 \times 10^4$ cm^{-6} pc. For unresolved H II regions, which is more likely, the detection limit corresponds to a minimum Lyman continuum flux. If there is no direct *uv* dust absorption, the Lyman continuum rate is

$$N_{\mathrm{Lyc}} = 1.1 \times 10^{50}\ \mathrm{s}^{-1}(S_{6\,\mathrm{cm}}/\mathrm{mJy})(D/\mathrm{Mpc})^2\ .$$

If the regions are optically thick or there is significant *uv* dust absorption, we will underestimate N_{Lyc}. Our detection limit of 4 σ at 2 cm corresponds to $N_{\mathrm{Lyc}} \sim 8 \times 10^{50}\ \mathrm{s}^{-1}$ at the 3.2 Mpc distance of our nearest galaxy; this corresponds to a few O4 stars, roughly as luminous as the largest Galactic H II regions, W49 and W51. H II regions that are detectable in the radio are far more luminous than those detectable in Hα (Kennicutt 1988; Kennicutt, Keel, & Blaha 1989). Lyman continuum rates that we obtain are listed in Table 5.

From N_{Lyc} we estimate properties of the starforming regions under the assumption of an initial mass function (IMF). By definition this type of analysis does not take into account evolution of the starburst, which introduces another parameter, the starburst age (e.g., Scoville & Soifer 1991). However, here we are most interested in the luminosity, number of OB stars, and mass consumption rates, which are dominated by the young stars. This analysis is also appropriate if the star formation favors massive stars, which appears to be the case in the most active galaxies (Rieke 1990). Aside from evolution, the biggest uncertainties in this procedure are in the choice of mass cutoffs for the IMF. Differences among various IMFs (e.g., Miller & Scalo 1979; Salpeter 1955; Van Buren 1985) pale by

TABLE 5

DERIVED STAR FORMATION PARAMETERS

	DERIVED[a]				OBSERVED[b]		
GALAXY	N_{Lyc} (10^{51} s^{-1})	M_{OB} ($10^5\ M_\odot$)	N_{OB} (10^3)	L_{OB} ($10^7\ L_\odot$)	L_{FIR} ($10^7\ L_\odot$)	(SN RATE)$^{-1}$[c] (yr)	$\dot{M}_{\mathrm{OB}}$ ($M_\odot$ yr^{-1})
Maffei 2	55	60	400	300	420	20	0.3
NGC 2403	<1	<1	<8	<5	...	>1000	<0.01
NGC 4236	<1	<1	<8	<5	...	>1000	<0.01
NGC 4258	5.5	6	40	30	30	200	0.03
NGC 4736	5.5	6	40	30	30	200	0.03
NGC 4826	2.8	3	20	20	100	400	0.02
M51	25	30	200	200	250	40	0.2
M83	75	80	500	500	440	15	0.4
M101	<10	<10	<70	<100	<27	>110	<0.1

[a] Uncertainties in derived N_{Lyc} scale as the errors in the estimated thermal fluxes, which are therefore less than a factor of 2. Uncertainties in starburst parameters are also dependent on IMF and mass cutoff assumptions discussed in text.

[b] Rickard & Harvey 1984 for inner arcminute region. When a luminosity is not given, it is estimated from their 100 μm fluxes, for a 40 K dust temperature.

[c] Supernova rates and gas consumption rates are estimated from N_{Lyc} using the IMF assumptions described in the text and the main sequence lifetimes of Maeder 1983, 1991.

comparison. We adopt a Salpeter IMF with an upper mass limit of 70 $M_\odot$ and a lower mass cutoff of 8 $M_\odot$, corresponding to spectral types O6.5–B3 ("OB"). We adopt the stellar parameters of Panagia (1973) and the zero-age main sequence (ZAMS) mass-luminosity relation of Maeder & Meynet (1989). The derived starburst parameters are listed in Table 5.

The most reliable number from the IMF analysis is L_{OB}, for which we obtain $L_{OB}/N_{Lyc} = 7 \times 10^{-44}$ $L_\odot$ s. This is dominated by massive young stars unless the starburst is unusually lengthy. The uncertainty in L_{OB}, largely due to uncertainty in IMF, is a factor of 2. Stellar masses are estimated for the OB population using $M_{OB}/N_{Lyc} = 1 \times 10^{-46}$ $M_\odot$ s, with an uncertainty of a factor of 2 due to choice of IMF. The total stellar mass of the regions, including stars of all masses, is likely to be at least one order of magnitude higher than M_{OB}. For the number of massive stars we adopt $N_{OB}/N_{Lyc} = 7 \times 10^{-48}$ s, with an uncertainty of about a factor of 3 due to IMF. N_{OB} is of interest because it is related to the supernova rate. We have estimated the supernova rate from N_{Lyc} using the main sequence lifetimes of Maeder (1983, 1990), $R_{SN}/N_{Lyc} = 9 \times 10^{-55}$ yr^{-1} s, and the mass consumption rate, $\dot{M}/N_{Lyc} = 6 \times 10^{-54}$ $M_\odot$ yr^{-1} s, both of which are dominated by the OB stars.

5. STAR FORMATION PROPERTIES

We have detected thermal fluxes in six of the 10 galaxies. M81 is the only galaxy with a significant 2 cm flux that does not have obvious thermal emission, but a weak thermal source might not be apparent near this bright active nucleus. The strength of the star formation in the nuclear regions of these galaxies is unusual by Galactic standards. The starbursts in Maffei 2 and M83 are 10^2–10^3 times as luminous as the large Galactic H II regions, W51 and W49 (Harvey, Campbell, & Hoffman 1977; Rengarajan et al. 1984). These regions contain more than 10^5 massive young stars. The weakest source, in NGC 4826, is still one order of magnitude more energetic than the largest Galactic complexes.

There is a wide range in starburst luminosity in the sample, from $L_{OB} = 5 \times 10^9$ $L_\odot$ in M83 to $L_{OB} < 8 \times 10^7$ $L_\odot$ in NGC 4236 and NGC 2403. The observations appear to rule out a strict correlation with Hubble type. For example, although the strongest sources happen to be Sbc galaxies, within the Sbc classification there is over two orders of magnitude of scatter in L_{OB}. This scatter appears within a sample selected to exhibit radio activity, so presumably the scatter is even larger in the general spiral population. There is no obvious correlation of nuclear star formation with total galactic blue luminosity, L_B (Table 1), and, presumably, with galactic mass.

The L_{OB} inferred from the thermal fluxes agree well with observed infrared luminosities, L_{IR}. The L_{IR} listed in Table 5 are from the survey of Rickard & Harvey (1984), whose arcminute beam matches our mapped regions. In all but one case, L_{OB} is in agreement with L_{IR}, given the uncertainties. With the possible exception of NGC 4286 (§ 6.2), the high infrared luminosities seen in the centers of these galaxies are likely to be due to star formation.

5.1. *Star Formation Efficiency: Comparison with the Molecular Gas*

The stellar masses produced by these starbursts range from $\sim$0.01–1 $M_\odot$ yr^{-1}, which would correspond, at a star formation efficiency of 30%, to gas consumption rates of $\sim$0.03–3 $M_\odot$ yr^{-1}. In the most active galaxies, the observed central molecular mass of a few 10^8 $M_\odot$ would be consumed within $\sim 10^8$ yr, which is short compared to the lifetime of the galaxy.

Related to the duration of the starburst is the quantity L_{OB}/M_{H_2}, a measure of the rate of star formation. L_{OB}/M_{H_2} is usually taken to be L_{IR}/M_{H_2} (e.g., Young & Scoville 1991); however, consideration of L_6/M_{H_2}, where L_6 is the 6 cm spectral luminosity ($L_6 = 4\pi D^2 S_6\, \nu$) is illuminating. In terms of the 6 cm flux, S_6,

$$\frac{L_6}{M_{H_2}} = 7\left(\frac{S_6}{10\ \mathrm{mJy}}\right)\left(\frac{S_{CO}}{1000\ \mathrm{Jy\ km\ s^{-1}}}\right)^{-1}\frac{L_\odot}{M_\odot},$$

for a Galactic conversion factor $N_{H_2}/I_{CO} = 3 \times 10^{20}$ cm^{-2} (K km s^{-1})$^{-1}$ (Scoville & Sanders 1987). We use CO fluxes from published single-dish observations from the NRAO 12 m telescope and the FCRAO 14 m telescope, whose beams closely match the mapped regions. We have also included the previously observed galaxies IC 342, NGC 253, and NGC 6946 (Turner & Ho 1983).

In Figure 3*a*, single-dish 6 cm fluxes are plotted versus CO fluxes, S_{CO}. Although the beams are not well matched, the CO flux is likely to be dominated by the innermost region where the radio continuum is concentrated. The correlation of single-dish ratio continuum flux with CO flux is weak. The amount of scatter suggests that the single-dish 6 cm continuum emission is not directly related to the recent star formation, but is representative of a longer term star-formation history. The values of L_6/M_{H_2} are high because we are including a large amount of synchrotron emission in L_6.

By contrast, the total 6 cm fluxes of the VLA maps are well correlated with S_{CO} (Fig. 3*b*). Unlike single-dish 6 cm fluxes, which are dominated by extended disk emission, the bright component of the VLA maps, although nonthermal, is likely to be directly associated with the recent star formation, as discussed above. The good correlation of the bright continuum emission with CO emission may be additional evidence for this result.

The 6 cm thermal fluxes, S_6^t, are plotted against S_{CO} in Figure 3*c*. Interestingly, the thermal fluxes are not as well correlated with the molecular masses as are the total mapped fluxes, which are largely synchrotron emission. The scatter in Figure 3*c* is not simply due to errors in estimating the thermal radio fluxes, since S_{IR}/S_{CO} shows similar scatter. Much of the scatter in S_6^t/S_{CO}, or L_6^t/M_{H_2}, is likely to reflect differences in the rates of recent star formation. If we take L_6^t as a measure of L_{OB}, we find that L_{OB}/M_{H_2} ranges from less than 1 $L_\odot/M_\odot$ to more than 20 $L_\odot/M_\odot$ (M83). This range is typical of Galactic molecular clouds, in which $L_{IR}/M_{H_2} \sim 1$ $L_\odot/M_\odot$ for quiescent clouds to $L_{IR}/M_{H_2} \sim$ 10–40 $L_\odot/M_\odot$ for clouds with H II regions (Scoville & Good 1989). These values of L_{OB}/M_{H_2} are averaged over roughly the inner kiloparsec of these galaxies, and on smaller scales L_{OB}/M_{H_2} may be higher. In fact, the highest L_{OB}/M_{H_2} in the plot are for the closest galaxies, so some of the scatter may be due to resolution effects.

5.2. *Relation of the Thermal and Nonthermal Radio Continuum Components*

In the galaxies with significant thermal fluxes, we have seen that the brightness of the nonthermal emission is consistent with the idea that the synchrotron emission in these maps is from young SNRs and RSNs directly associated with recent star formation. The morphology is also consistent with this result, as will be discussed for individual galaxies in § 6.2. We

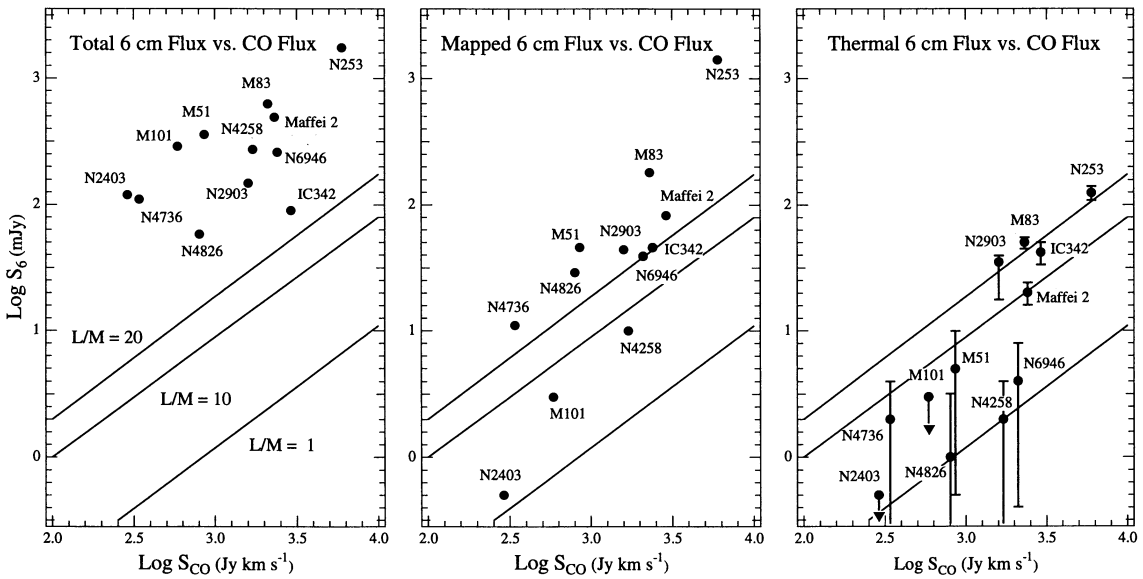

FIG. 3a FIG. 3b FIG. 3c

FIG. 3.—6 cm fluxes versus CO flux. CO data from Adler & Liszt (1989), Blitz, Mathieu, & Bally (1986), Combes et al. (1977), Elmegreen & Elmegreen (1982), Kenney et al. (1991), Rickard, Turner, & Palmer (1984), Sanders & Mirabel (1985), Scoville & Young (1983), Solomon et al. (1983), and Young & Scoville (1982). (*a*) Single dish 6 cm fluxes; (*b*) total mapped 6 cm fluxes (this paper); (*c*) estimated thermal (free-free) fluxes (this paper).

now consider whether the relative amounts of thermal to nonthermal emission are consistent with the idea that the synchrotron emission arises in young SNRs and RSNs associated with recent star formation.

Are the synchrotron fluxes for these galaxies consistent with the estimated star-formation rates? Unfortunately, the amount of radio emission from an SNR depends critically on its environment (e.g., Chevalier 1990), which produces the range of three to four orders of magnitude in spectral luminosity of Galactic SNRs (Green 1984). Therefore we can only make a general consistency argument, similar to that of Ulvestad (1982) for Seyfert galaxies. If we adopt a mean 6 cm spectral luminosity of $\langle L_6^{nt} \rangle = 3 \times 10^{17}$ W Hz^{-1} for a "typical" SNR, the observed nonthermal luminosities (Table 4) imply the presence of ~40–900 SNR in each galaxy. We can test the reasonableness of this result by calculating the lifetimes of the SNR required to explain the observed SNR numbers, given the inferred supernova rates (Table 5). Mean lifetimes are $\tau_{SNR} = L_6^{nt}/R_{SN}\langle L_6^{nt} \rangle$. Excluding galaxies with active nuclei, we obtain $\tau_{SNR} \sim$ 15,000–20,000 yr. These lifetimes are similar to those estimated for Galactic SNRs. The consistency of the observed nonthermal luminosities with typical luminosities and lifetimes of Galactic SNRs suggests that star formation could be responsible for the bright synchrotron emission. Monitoring of these galaxies will further constrain the supernova rates.

The relative percentages of thermal and nonthermal flux in these galaxies varies significantly. The thermal fraction is 3%–30% at 6 cm, and 10%–60% at 2 cm. The large range observed is clearly related to the wide variation in spectral index that is observed within the VLA maps (Tables 2 and 4; Fig. 2). This suggests that RSNs and young SNRs, which have variable flux and spectral index over timescales short compared to the star formation timescales, dominate the observed bright emission. A single RSN (see Sramek & Weiler 1990) can appreciably affect the total flux in even the most luminous of the galaxies, and its flux and spectral index will change radically on a timescale of tens of years.

6. INDIVIDUAL GALAXIES

Consideration of the circumstances unique to each of the galaxies can shed light on the sources of the radio continuum and its relation to the galaxy as a whole. We have separated the galaxies in the following discussion in three groups: those without bright continuum emission, those dominated by nuclear star formation, and those with likely AGN activity.

6.1. *The Quiet Galaxies*

Three galaxies have little radio continuum emission with the central arcminute: NGC 2403, NGC 4236, and M101. It is perhaps not a coincidence that the least luminous galaxies in the sample, NGC 2403 and NGC 4236, fall in this group. However, M101, the most luminous galaxy, has little continuum emission. There is no obvious property of these galaxies that might explain why they are devoid of nuclear continuum emission, except perhaps that none of these galaxies shows evidence for a prominent bar.

1. *NGC 2403.*—NGC 2403 is an Scd galaxy similar to M33. Like M33, it has little nuclear continuum emission. The brightest sources in NGC 2403 form a double source at $7^h32^m17^s.84/18^s.91$, 65°43′21″.2/20″.3. This is probably a background radio galaxy. The other sources are very weak; sources 3, 5, and 6 show extended emission that may be related to star formation. Source 1 (Table 2; not shown in Fig. 1*b*) is a shell source of diameter 7″ (100 pc) that may be an SNR.

2. *NGC 4236.*—NGC 4236 is another dwarf spiral with no nuclear continuum emission. The observed sources are unresolved and possibly RSNs or SNRs, although the positive spectral index, $\alpha = +0.5$, of source 1 suggests that it may be the core of a background radio galaxy or quasar.

3. *M101.*—M101 has a weak extended continuum source at the position of the nucleus with a 6 cm flux of 3 mJy. We did not observe M101 at 2 cm, so there is no spectral index for this source. The upper limit to the infrared luminosity for this region of 2.8×10^8 $L_\odot$ implies that free-free emission consti-

tutes less than 30% of the 6 cm flux. This is also consistent with the relatively small amount of CO observed toward the nucleus (Kenney, Scoville, & Wilson 1991).

6.2. *The Starburst Galaxies*

1. *Maffei 2.*—Maffei 2 has a sizeable starburst in its core. With $L_{IR} = 4 \times 10^9\ L_\odot$ (Rickard & Harvey 1984), it has an infrared luminosity within a factor of two of NGC 253 or M82. Maffei 2, unhappily, is located in the Galactic plane ($b = -0.^\circ5$) behind ~ 5 magnitudes of visual extinction (Spinrad et al. 1973; Buta & McCall 1983). Radio continuum emission was first observed in the nucleus by Seaquist, Pfund, & Bignell (1976), and their slightly lower resolution maps look very much like ours. Maffei 2 appears to be an interacting galaxy, from its strongly barred appearance evident in recent near-infrared images (Hurt et al. 1992). The bar may facilitate the flow of gas from the disk into the nucleus (e.g. Athanassoula 1992), causing the star formation there.

Maps of the thermal and nonthermal radio continuum emission in Maffei 2 are presented in Figure 4. These maps were produced as described in § 3.1, with an adopted nonthermal spectral index of -0.75. The thermal emission (Fig. 4*a*) consists of a series of clumps, aligned in the north-south direction. These H II regions can also be seen as peaks in the spectral index map (Fig. 2*a*) The nothermal emission in Figure 4*b* generally follows the structure of the H II regions, although it also appears to extend farther to the south that the thermal sources. The nonthermal emission is clearly associated with the star formation and peaks up on the centroid of the thermal emission, but the synchrotron component appears to be more diffuse and extended. It is interesting that the 10 μm source in Maffei 2 (Ho et al. 1989; Telesco et al. 1993) appears to follow the synchrotron component more closely than the H II regions, leading Ho et al. to suggest that the 10 μm emission originates from warm dust in shock-heated regions. The diffuse nature of the nonthermal component in Maffei 2 might be expected for SNRs in the process of expanding and merging with the general ISM.

The pattern of star formation in the nucleus of Maffei 2 displays a coherence that is unlikely to result from the internal effects such as sequential star formation (e.g., Elmegreen & Lada 1978). The minimum crossing time of the kiloparsec-sized continuum source is $\gtrsim 10^8$ yr for a maximum sound speed of 10 km s^{-1}, far longer than the lifetimes of the OB stars and probably the starburst as well. Comparison with interferometric CO observations suggests that a likely reason for the alignment is the distribution of molecular gas. The CO emission in the center of Maffei 2 is distributed along two open spiral arms, forming a barlike structure as viewed from the inclination of 66° (Ishiguro et al. 1989). The radio continuum source is located at the southern end of the northern CO arm, just above the central cavity observed by Ishiguro et al. The morphology of the star formation traced by the radio continuum closely follows the morphology of the molecular gas (Hurt & Turner 1991). The presence of the starburst in Maffei 2 is due not to unusually high star-formation efficiencies, but to the presence of large amounts of molecular gas.

2. *NGC 4826.*—NGC 4826 is the only galaxy in this sample for which the free-free luminosity is inconsistent with its observed infrared luminosity (Table 5). This galaxy produces too much infrared luminosity for its observed radio flux. Only if all of the 2 cm flux observed in NGC 4826 were thermal, which it is not (Fig. 2*b*), would the predicted L_{OB} equal the observed L_{IR}. NGC 4826 also has very high nonthermal fraction, 97% at 6 cm and 11% at 2 cm. Either the OB stellar population is not radio dominant at the moment because the starburst is very young, and the H II regions are optically thick, or else the starburst has stopped, leaving only nonionizing stars. Another possibility is that RSNs are for some reason more common in NGC 4826 than in other galaxies.

3. *M83.*—M83 has very active star formation in its core. The nuclear infrared luminosity is $4 \times 10^9\ L_\odot$ (Rickard & Harvey 1984), similar to that of Maffei 2. Previous radio continuum maps of M83 appear in Condon et al. (1982), Cowan & Branch (1985), and Ondrechen (1985). Our separation of the thermal and nonthermal emission is presented in Figure 5. We

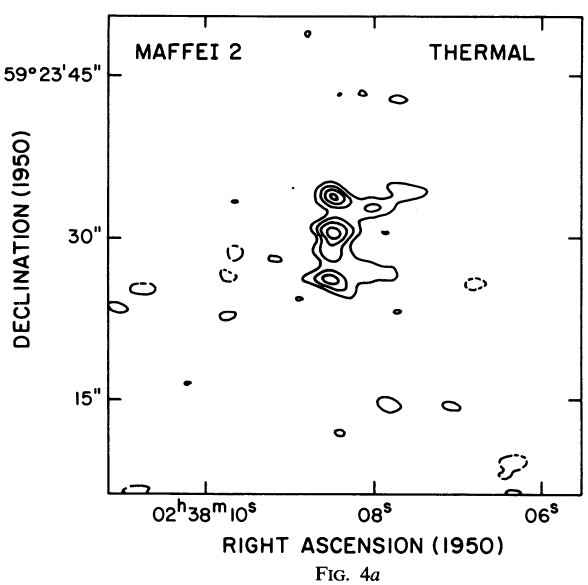

FIG. 4*a*

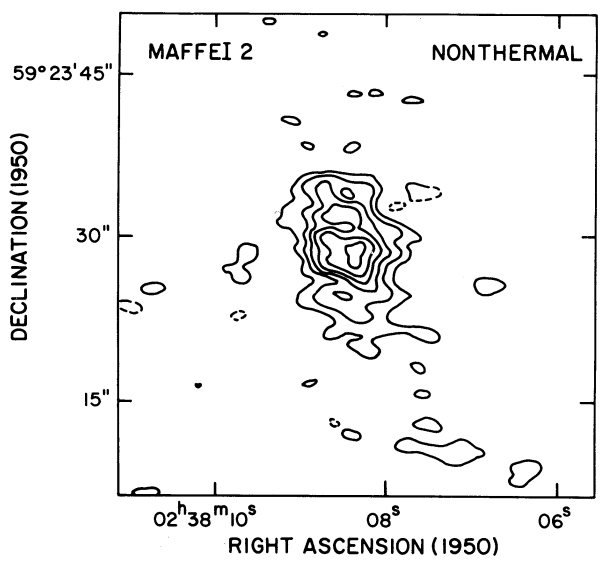

FIG. 4*b*

FIG. 4.—Spectral separation of Maffei 2 into flat spectrum and steep spectrum components, using the 6 cm and 2 cm maps and assuming $\alpha = -0.1$ for the flat component and $\alpha = -0.8$ for the steep component. The flat component is a representation of the likely structure of the thermal bremsstrahlung (free-free) component of the continuum, while the steep spectrum emission is nonthermal synchrotron emission from SNRs. Contours are multiples of 0.8 mJy beam^{-1}. (*a*) Thermal component of Maffei 2; (*b*) nonthermal component of Maffei 2.

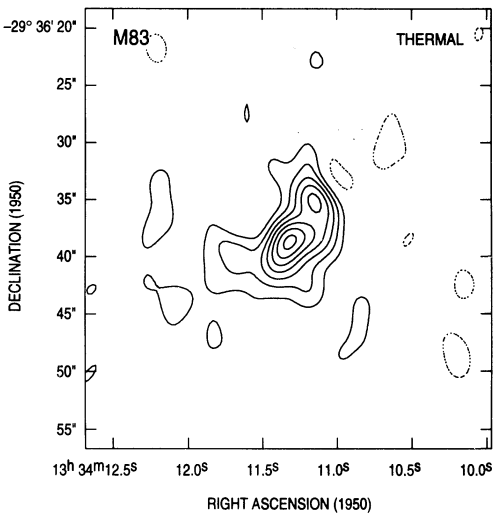

FIG. 5a

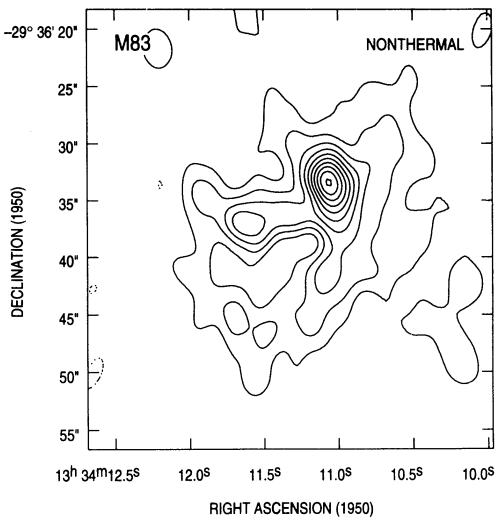

FIG. 5b

FIG. 5.—Spectral separation of M83 into flat spectrum and steep spectrum components, using the 6 cm and 2 cm maps and assuming $\alpha = -0.1$ for the flat component and $\alpha = -0.8$ for the steep component. The flat component is a representation of the likely structure of the thermal bremsstrahlung (free-free) component of the continuum, while the steep spectrum emission is nonthermal synchrotron emission from SNR. Contour levels are multiples of 1 mJy beam^{-1}. (*a*) Thermal component of M83; (*b*) nonthermal component of M83. The strong compact component to the NW of the nucleus is possibly the radio counterpart of SN 1968K.

adopted a nonthermal spectral index of $\alpha_{nt} = -0.8$ for the separation, which is also the spectral index observed in the lower resolution maps of Ondrechen.

The thermal emission in M83, depicted in Figure 5*a*, is in excellent agreement with the observed 10 μm structure (Telesco 1988; Telesco et al. 1993). The arclike structure of H II regions is located at the end of one of the two CO arms coming into the nucleus (Handa et al. 1990; Turner, Kenney, & Hurt 1993). The thermal arc is offset by $\sim 5''$ from the northern CO peak to the northwest. A curious feature of the thermal emission in M83 is that it may be optically thick. This conclusion was reached by Turner, Ho, & Beck (1987) on the basis of the comparison of the relative strength of the Brackett recombination lines and the thermal radio continuum. This result is independent of the thermal/nonthermal separation since not even the total observed radio continuum flux is sufficient to produce "normal" Brackett/radio flux ratios. Optically thick galactic H II regions tend to be very small, 0.1 pc diameter or less, so it is unusual that a region of few hundred parsecs across, such as we observe in M83, could be entirely optically thick. This interpretation would appear to require that the H II regions in M83 be very young, $\lesssim 10^4$ yr. An alternative explanation for this result is that the radio emission is produced by optically thick emission from young stellar objects (Thompson 1987), although it would again require an unusually high number of these very young sources.

The nonthermal emission in M83 is more extended and diffuse than the thermal component, and is centered on the thermal source (Fig. 5*b*), as in Maffei 2. The weaker continuum emission follows the CO arms (Turner, Kenney, & Hurt 1993).

The nonthermal separated map of Figure 5*b* reveals a particularly strong compact source that is not apparent in the 6 cm map, owing to confusion. This component, also visible in the 21 cm map of Condon et al. (1982), is located at $\alpha = 13^h34^m11^s.06$, $\delta = -29°36'33''.5$. The deconvolved size of the source is $< 5''$, or 120 pc, and it has a brightness temperature of ~ 60 K. The spectral index is -0.8. Given the high brightness, steep spectrum and compact nature, this source is a good candidate for an RSN. In fact, this source is located very close to the position of the optical supernova, SN 1968L. This supernova was identified as Type II and located 2″–3″ west of the optical center by Wood & Andrews (1974). We located our compact radio source about 6″ to the west and 7″ north of the optical center as given in Rumstay & Kaufman (1983). Given the difficulty of assigning an optical center in this dusty and confused region, the identification of this source with SN 1968L is possible. Confirmation will require a radio light curve.

6.3. *The AGN Candidates*

1. *M51.*—In the galaxies with AGN candidates there is often some suggestion that the observed large-scale continuum structure is related, either directly or indirectly, to the nuclear source. The large "bubble" to the north of the nuclear source in M51 is an example (Ford et al. 1985). This bubble has a diameter of ~ 300 pc. It seems unlikely that a SNR could maintain a clear shell structure until it reached this size. The source immediately to the south of the nuclear source has a flat spectrum, as evident from Figure 1*i* and 2*d*. N II line profiles in the southern source indicate unusually high velocities (Cecil 1988). We see a flat radio spectrum in this southern source, from which we infer thermal flux, which would be consistent with the observed far-infrared luminosity (Table 5). However it is also possible that this radio source is synchrotron emission from the working surface of a weak jet. The fact that the spectral index flattens toward the side away from the nucleus would also support this hypothesis, which is discussed at length by Cecil.

2. *NGC 4258.*—NGC 4258 appears to have an active nucleus. The nucleus has a weak broad line region in the optical (Stauffer 1982) with H_2O megamasers (Claussen, Heiligman, & Lo 1984). The large-scale structure of the galaxy is also peculiar, with a set of anomalous Hα and radio continuum arms offset from the stellar arms (van der Kruit, Oort, & Mathewson 1972; van der Kruit 1974; van Albada & van der Hulst 1982; Ford et al. 1986). There is bright compact continuum emission along the anomalous arms (Fig. 1*f*). The arms are not detectable at 2 cm, so we do not have spectral indices for these sources.

Numerous authors, beginning with van der Kruit, Oort, &

Mathewson (1972) have suggested that the anomalous arms in NGC 4258 arise through some form of nuclear ejection. The kinematics of the ionized gas seem to support this idea (Rubin & Graham 1990; Cecil, Wilson, & Tully 1992). A high-resolution CO map of the nucleus (Martin et al. 1989; Plante et al. 1991) shows that the molecular gas is anticorrelated with the Hα "jet" (Cecil et al. 1992) connecting the arms. Plante et al. suggest that the Hα traces a jet channel evident as a gap in the molecular gas. We find that the bright continuum source in the center of NGC 4258 (Fig. 1*e*) is indeed located in the "channel" between the two CO lobes of the Plante et al. map, offset by about 5″ from the CO arm. The nuclear continuum source is very bright, with $T_b > 2000$ K, and has an inverted spectrum ($\alpha = +0.4$) suggestive of an opaque synchrotron core source. However, the faint emission in the 6 cm map to the south and west of the nucleus does not form part of the Hα "jet" but is coincident with the brighter of the CO arms, at a position angle of $-30°$. The CO peak is located at the gap in this low-level continuum structure. The presence of continuum emission coincident with the molecular arms in the nucleus invokes the possibility that extinction causes the apparent anticorrelation of the CO and Hα features in the nucleus, rather than the channel left by a jet.

In NGC 4258, the compact source to the north of the nucleus has been identified as SN 1981K, the first radio-detected supernova (van der Hulst et al. 1983b). The 6 cm flux of 1 mJy, is consistent with the radio light curve, and in fact, this appears to be the earliest 6 cm flux for this source. When combined with the 20 cm flux for that date (van der Hulst et al. 1983b), we obtain a spectral index of $\alpha = -0.8$, which is flatter than subsequent spectral indices (Weiler et al. 1986). The steepening of spectral index with time is often observed in RSNs (Weiler & Sramek 1988).

3. *NGC 4736.*—NGC 4736 has a large continuum "ring" of diameter 2 kpc (Fig. 1*g*), discussed by Duric & Dittmar (1988). This ring is also seen in Hα (Buta 1988; Pogge 1989) and the far-infrared (Smith et al. 1991). It is unclear if this is really a ring or simply very circular spiral arms (Buta 1988). The compact radio continuum structures within the ring tend to have flat spectra (Table 2) and are likely to be very active star-forming regions of the W51/W49 variety. The total 6 cm flux for the ring is 41 mJy, and the 2 cm flux is 27 mJy. The estimated total thermal flux for the sources in the ring at 6 cm is 13 mJy, with a corresponding OB luminosity of $L_{OB} = 2.5 \times 10^9\ L_\odot$. This is in agreement with the far-infrared luminosity of the ring, $L_{IR} = 2 \times 10^9\ L_\odot$ (Smith et al. 1991, corrected for distance). It is thus likely that most of the far-infrared luminosity is produced in the H II regions that we see in the radio maps.

Van der Kruit (1974, 1976) and Sanders & Bania (1976) suggested that the ring in NGC 4736 formed from an explosive nuclear event. Our observations do suggest the presence of an AGN, since the very compact nuclear source has a 6 cm brightness temperature of $\gtrsim 1000$ K (Table 3). This is consistent with the Liner spectral classification (Heckman, Balick, & Crane 1980). Aside from the compact core source, there is little nuclear continuum emission and no indication of any connection between the ring and the nucleus. We estimate a 6 cm thermal flux of 2 mJy, or $L_{OB} = 4 \times 10^8\ L_\odot$ for the central arcminute of NGC 4736, from the region 5″–10″ south of the nucleus. This is less than the observed far-infrared luminosity of $L_{IR} = 1.3 \times 10^9\ L_\odot$ for the same region (Smith et al. 1991, corrected for distance). The lack of thermal radio continuum in the nucleus is also consistent with the absence of Hα emission there (Smith et al.). The additional far-infrared luminosity originates either in non-OB stars from an aged starburst (Walker, Lebofsky, & Rieke 1988) or in the nonthermal core source.

7. CONCLUSIONS

From a sample of 10 nearby large spiral galaxies, we detect bright radio continuum emission of brightness temperature T_b(6 cm) ~ 1–90 K in eight. The mapped 6 cm emission on these size scales (1.″5; ~20–50 pc) is largely nonthermal synchrotron emission. The high intensity of the emission requires that the compact 6 cm emission generally originates in relatively young SNRs or RSNs directly associated with star formation and not in an extended disk component as seen at lower resolution. Four of the galaxies (NGC 3031, NGC 4258, NGC 4736, and M51) have high-brightness sources coincident with the dynamical centers that are likely to be slightly more luminous versions of the Galactic source Sgr A*. In M51 and NGC 4258 there is evidence that the larger scale continuum structure may also be caused by nuclear activity.

From our spectral separation of the thermal and nonthermal emission components in the starforming galaxies, we find that the percentage of the total continuum emission that is due to thermal free-free emission ranges from 3%–30% at 6 cm, and 10%–60% at 2 cm. Where the regions are well resolved, it can be seen that the thermal and nonthermal components have slightly different spatial distributions, with the nonthermal component more diffuse and extended. From the derived thermal fluxes, we derive Lyman continuum rates and estimates of the total luminosities due to massive young stars. We detect a range of activity corresponding to $N_{Lyc} = 3 \times 10^{51}$ s^{-1} in NGC 4826 to $N_{Lyc} = 8 \times 10^{52}$ s^{-1} in M83. The corresponding range of young stellar luminosities is $L_{OB} \sim 2 \times 10^8$ to $5 \times 10^9\ L_\odot$. The derived L_{OB} are in agreement with observed far-infrared luminosities. In all galaxies the star formation efficiencies are similar to galactic values as determined by the total mass of molecular gas.

The observed nonthermal luminosities are consistent with the expectation that even the nonthermal emission in these maps is directly associated with recent star formation. We also identify a number of RSN candidates, including a possible counterpart to SN 1968L in the nucleus of M83. The fact that young SNR and RSN, with rapidly changing fluxes and spectral indices, are likely to contribute significantly to the fluxes may explain the wide range in radio continuum properties that is observed at this resolution.

The authors with to thank an anonymous referee for helpful comments. This work was supported by NSF grants AST 87-20759 (P. T. P. H.) and AST 90-22996 (J. L. T.).

REFERENCES

Adler, D. S., Allen, R. J., & Lo, K. Y. 1991, ApJ, 382, 475
Adler, D. S., & Liszt, H. S. 1989, ApJ, 339, 836
Athanassoula, L. 1992, MNRAS, 259, 345
Baars, J. W. M., Genzel, R., Pauliny-Toth, I. I. K., & Witzel, A. 1977, A&A, 61, 99
Bartel, N., et al. 1987, ApJ, 323, 505
Bash, F. N. 1986, private communication
Bash, F. N., & Kaufman, M. 1986, ApJ, 310, 621
Becklin, E. E., Gatley, I., Matthews, K., Neugebauer, G., Sellgren, K., Werner, M. W., & Wynn-Williams, C. G. 1980, ApJ, 236, 441

Blitz, L., Mathieu, R. D., & Bally, J. 1986, ApJ, 311, 142
Buta, R. J. 1988, ApJS, 66, 233
Buta, R. J., & McCall, M. L. 1983, MNRAS, 205, 131
Caesarsky, C. J. 1980, ARA&A, 18, 289
Cecil, G. 1988, ApJ, 329, 38
Cecil, G., Wilson, A. S., & Tully, R. B. 1992, ApJ, 390, 365
Chevalier, R. A. 1982, ApJ, 259, 302
———. 1990, in Massive Stars in Starbursts, ed. C. Leitherer, N. R. Walborn, T. M. Heckman, & C. A. Norman (Cambridge: Cambridge Univ. Press), 169
Clark, D. H., & Caswell, J. L. 1976, MNRAS, 174, 267
Claussen, M. J., Heiligman, G. M., & Lo, K. Y. 1984, Nature, 310, 298
Combes, F., Encrenaz, P. J., Lucas, R., & Weliachew, L. 1977, A&A, 55, 311
Condon, J. J. 1983, ApJS, 53, 459
———. 1987, ApJS, 65, 485
Condon, J., Condon, M. H., Gisler, G., & Puschell, J. 1982, ApJ, 252, 102
Cowan, J. J., & Branch, D. 1985, ApJ, 293, 400
de Bruyn, A. G. 1977, A&A, 54, 491
de Jong, M. L. 1967, ApJ, 150, 1
de Jong, T., Klein, U., Wielebinski, R., & Wunderlich, E. 1985, A&A, 147, L6
Dickey, J., & Salpeter, E. 1984, ApJ, 284, 461
Dressel, L. L., & Condon, J. J. 1976, ApJS, 31, 187
Duric, N. 1986, ApJ, 304, 96
Duric, N., Seaquist, E. R., Crane, P. C., & Davis, L. E. 1986, ApJ, 304, 82
Duric, N., & Dittmar, M. R. 1988, ApJ, 332, L67
Duric, N., Seaquist, E. R., Crane, P. C., Bignell, R. C., & Davis, L. E. 1983, ApJ, 273, L11
Ekers, R. D. 1975, in Structure and Evolution of Galaxies, ed. S. Setti (Dordrecht: Reidel), 217
Ekers, R. D., et al. 1989, MNRAS, 236, 737
Elmegreen, B. G., & Lada, C. J. 1978, ApJ, 214, 725
Elmegreen, D. M., & Elmegreen, B. G. 1982, AJ, 87, 626
Ford, H. C., Crane, P. C., Jacoby, G. H., Lawrie, D. G., & van der Hulst, J. M. 1985, ApJ, 293, 132
Ford, H. C., Dahari, O., Jacoby, G. H., Crane, P. C., & Ciardullo, R. 1986, ApJ, 311, L7
Gioia, I. M., Gregorini, L., & Klein, U. 1982, A&A, 116, 164
Gavazzi, G., Cocito, A., & Vettolani, G. 1986, ApJ, 305, L15
Goss, W. M., Kalbera, P. M. W., & Dickel, H. R. 1984, A&A, 139, 317
Green, D. B. 1984, MNRAS, 209, 449
Habing, H. J., & Israel, F. P. 1979, ARA&A, 17, 345
Handa, T., Nakai, N., Sofue, Y., Hayashi, M., & Fujimoto, M. 1990, PASJ, 42, 1
Harvey, P. M., Campbell, M. H., & Hoffman, W. F. 1977, ApJ, 211,786
Heckman, T. M., Balick, B., & Crane, P. C. 1980, A&AS, 40, 295
Helou, G., Soifer, B., & Rowan-Robinson, M. 1985, ApJ, 298, L7
Ho, P. T. P., Turner, J. L., Fazio, G. G., & Willner, S. P. 1989, ApJ, 344, 135
Hummel, E., Pedlar, A., van der Hulst, J. M., & Davies, R. D. 1985, A&AS, 60, 293
Hurt, R. L., Merrill, K. M., Gatley, I., & Turner, J. L. 1992, AJ, 105, 121
Hurt, R. L., & Turner, J. L. 1991, ApJ, 377, 434
Ishiguro, M., et al. 1989, ApJ, 344, 763
Israel, F. P., & van der Hulst, J. M. 1983, AJ, 88, 1736
Kellerman, K. I., Shaffer, D. B., Pauliny-Toth, I. I. K., Preuss, E., & Witzel, A. 1976, ApJ, 210, L121
Kenney, J. D. 1992, private communication
Kenney, J. D. P., Scoville, N. Z., & Wilson, C. D. 1991, ApJ, 366, 432
Kennicutt, R. C. 1988, ApJ, 334, 144
Kennicutt, R. C., Keel, W. C., & Blaha, C. A. 1989, AJ, 97, 1022
Keto, E., Ball, R., Arens, J., Jernigan, G., Meixner, M., Skinner, C., & Graham, J. 1993, ApJ, 411, 266
Klein, U., & Emerson, D. T. 1981, A&A, 94, 29
Kronberg, P. P., Bierman, P., & Schwab, F. R. 1985, ApJ, 291, 693
Lebofsky, M. J., & Rieke, G. H. 1979, ApJ, 229, 111
Maeder, A. 1993, A&A, 120, 113
———. 1991, in Massive Stars in Starbursts, ed. C. Leitherer, N. R. Walborn, T. N. Heckman, & C. A. Norman (Cambridge: Cambridge Univ. Press), 97
Maeder, A., & Meynet, G. 1989, A&A, 210, 155
Martin, P., Roy, J.-R., Noreau, L., & Lo, K. Y. 1989, ApJ, 345, 707
Mathewson, D. S., van der Kruit, P., & Brouw, W. N. 1972, A&A, 17, 468
McKee, C. F. 1989, ApJ, 345, 782
Miller, G. M., & Scalo, J. M. 1979, ApJS, 41, 513
Mills, B. Y., Turtle, A. J., Little, A. G., & Durdin, J. M. 1984, Australian J. Phys., 37, 321
Ondrechen, M. P. 1985, AJ, 90, 1474
Panagia, N. 1973, AJ, 78, 929
Plante, R. L., Lo, K. Y., Roy, J.-R., Martin, P., & Noreau, L. 1991, ApJ, 381, 110
Pogge, R. 1989, ApJS, 71, 433
Rengarajan, T. N., Cheung, L. H., Fazio, G. G. Shivananadan, K., & McBreen, B. 1984, ApJ, 286, 573
Rickard, L. J, & Harvey, P. M. 1984, AJ, 89, 1520
Rickard, L. J, Turner, B. E., & Palmer, P. 1984, ApJ, 218, L51
Rieke, G. H. 1990, in Massive Stars in Starbursts, ed. C. Leitherer, N. R. Walborn, T. M. Heckman, & C. A. Norman (Cambridge: Cambridge Univ. Press), 205
Rieke, G. H., Lebofsky, M. J., Thompson, R. I., Low, F. J., & Tokunaga, A. T. 1980, ApJ, 238, 24
Roche, P. F., & Aitken, D. K. 1985, MNRAS, 213, 789
Rubin, V. C., & Graham, J. A. 1990, ApJ, 362, L5
Rumstay, K. S., & Kaufman, M. 1983, ApJ, 274, 611
Salpeter, E. E. 1955, ApJ, 121, 161
Salter, C. J., & Brown, R. L. 1988, in Galactic and Extragalactic Radio Astronomy, ed. G. L. Verschuur & K. I. Kellerman (New York: Springer-Verlag), 1
Sanders, D. B., & Mirabel, I. F. 1985, ApJ, 298, L31
Sanders, R. H., & Bania, R. M. 1976, ApJ, 204, 34
Scalo, J. M. 1986, Rev. Cosmic Phys., 11, 1
Scoville, N. Z., & Good, J. C. 1989, ApJ, 399, 149
Scoville, N. Z., & Sanders, D. N. 1987, in Interstellar Processes, ed. D. J. Hollenbach & H. A. Thronson, Jr. (Dordrecht: Kluwer), 21
Scoville, N. Z., & Soifer, B. T. 1991, in Massive Stars in Starbursts, ed. C. Leitherer, N. R. Walborn, T. M. Heckman, & C. A. Norman (Cambridge: Cambridge Univ. Press), 233
Scoville, N. Z., & Young, J. S. 1983, ApJ, 265, 148
Seaquist, E. R., Pfund, J., & Bignell, R. C. 1976, A&A, 48, 413
Smith, B. J., Lester, D. F., Harvey, P. M., & Pogge, R. W. 1991, ApJ, 373, 66
Solomon, P. M., Barrett, J., Sanders, D. B., & de Zafra, R. 1983, ApJ, 266, L103
Spinrad, H., et al. 1973, ApJ, 180, 351
Sramek, R. 1975, AJ, 80, 771
Sramek, R., & Weedman, D. 1986, ApJ, 301, 640
Sramek, R., & Weiler, K. W. 1990, in Supernovae, ed. A. G. Petschek (New York: Springer-Verlag), 77
Stauffer, J. R. 1982, ApJ, 262, 166
Telesco, C. M. 1988, ARA&A, 26, 343
Telesco, C. M., Dressel, L. L., & Wolstencroft, R. D. 1993, ApJ, 414, 120
Thompson, R. I. 1987, ApJ, 321, 153
Tilanus, R. P. J., Allen, R. J., van der Hulst, J. M., Crane, P. C., & Kennicutt, R. C. 1988, ApJ, 330, 667
Tully, R. B. 1987, Nearby Galaxies Catalogue (Cambridge: Cambridge Univ. Press)
Turner, J. L., & Ho, P. T. P. 1983, ApJ, 268, L79
———. 1985, ApJ, 299, L77
Turner, J. L., Ho, P. T. P., & Beck, S. C. 1987, ApJ, 313, 644
Turner, J. L., Kenney, J., & Hurt, R. L. 1991, in preparation
Ulvestad, J. S. 1982, ApJ, 259, 96
van Albada, G. D., & van der Hulst, J. M. 1982, A&A, 115, 263
Van Buren, D. 1985, ApJ, 294, 567
van der Hulst, J. M., Crane, P. C., & Keel, W. C. 1981, AJ, 86, 1175
———. 1983a, AJ, 88, 138
van der Hulst, J. M., Hummel, E., Davies, R. D., Pedlar, A., & van Albada, G. D. 1983b, Nature, 306, 566
van der Hulst, J. M., Kennicutt, R. C., Crane, P. C., & Rots, A. H. 1988, A&A, 195, 38
van der Kruit, P. C. 1973a, A&A, 29, 231
———. 1973b, A&A, 29, 249
———. 1973c, A&A, 29, 263
———. 1974, ApJ, 192, 1
———. 1976, A&A, 52, 85
van der Kruit, P. C., Oort, J. H., & Mathewson, D. S. 1972, A&A, 21, 169
Visser, H. C. D. 1980, A&A, 88, 159
Walker, C. E., Lebofsky, M. J., & Rieke, G. H. 1988, ApJ, 325, 687
Weiler, K. W., Panagia, N., Sramek, R. A., van der Hulst, J. M., Roberts, M. S., & Nguyen, L. 1989, ApJ, 336, 421
Weiler, K. W., & Sramek, R. A. 1988, ARA&A, 26, 295
Weiler, K. W., Sramek, R. A., Panagia, N., van der Hulst, J. M., & Salvati, M. 1986, ApJ, 301, 790
Whiteoak, J. B. 1970, Astrophys. Lett., 5, 29
Wood, R., & Andrews, P. J. 1974, MNRAS, 167, 13
Wunderlich, E., Klein, U., & Wielebinski, R. 1988, A&AS, 69, 487
Wynn-Williams, C. G., & Becklin, E. E. 1985, ApJ, 290, 108
Young, J. S., & Scoville, N. Z. 1982, ApJ, 258, 467
———. 1991, ARA&A, 29, 581